INVESTIGATION OF COMPLEX MASS AND HEAT TRANSFER TRANSITIONAL PROCESSES OF DISPERSED WATER DROPLETS IN WET GAS FLOW IN THE FRAMEWORK OF HEAT UTILIZATION TECHNOLOGIES FOR BIOFUEL COMBUSTION AND FLUE GAS REMOVAL

G. Miliauskas [1], M. Maziukienė[1], H. Jouhara[2] and R. Poškas[1,3]

1. Department of Thermal and Nuclear Energy, Faculty of Mechanical Engineering and Design, Kaunas University of Technology, Kaunas, Lithuania; email: gintautas.miliauskas@ktu.lt
2. College of Engineering, Design and Physical Sciences, Institute of Energy Futures, Brunel University London, UK; email: Hussam.Jouhara@brunel.ac.uk
3. Nuclear Engineering Laboratory, Lithuanian Energy Institute, Kaunas, Lithuania; email: Robertas.Poskas@lei.lt

ABSTRACT

In this paper, complex processes of water droplet heat and mass transfer are analyzed in a cycle of condensing, transitional evaporation and equilibrium evaporation regimes during phase change which occurs on a droplet's surface. The dynamics of a heated droplet's surface temperature is directly related to the change in the regimes. The definition of the dynamics is based on a numerical iterative scheme which depends on the balance of a droplet surface's heat flux. In this scheme, the energy of phase change and external heat transfer are combined as well as the internal heat transfer occurring in droplets. The numerical investigation results of the water droplets' phase change were used as a basis while defining the inputs provided by the droplet slipping and the radiation absorbed in the flue gas within the interactions between the processes of complex transitional transfers. For this investigation, the conditions have been set to be typical for heat utilization technologies and biofuel furnaces used in flue gas removal.

Keywords: water droplets, convective radiative combine heating, condensation and transitional evaporation regimes of phase change, numerical modelling

Abbreviations: a is thermal diffusivity, m^2/s; B_T is Spalding transfer parameter; C_l is droplet drag coefficient; D is mass diffusivity, m^2/s; Fo is Fourier number; $\dot{m}$ is vapor mass flow rate, kg/s; I_ω is spectral intensity of radiation, W/(m steer); k_c is effective conductivity parameter; k_ω is spectral index of absorption; L is latent heat of evaporation, J/kg; m is vapor mass flux, kg/(m^{2}s); M is mass, kg; n_ω is spectral index of refraction; $\overline{n}_\omega$ is complex's spectral index of refraction; Nu is Nusselt number; p is pressure, Pa; P is symbol of free parameter in heat-mass transfer; Re is Reynolds number; Pr is Prandtl number; q is heat flux, W/m^2; r is radial coordinate, m; R is radius of a droplet, m; R_μ is universal gas constant J/(kmol K); T is temperature, K; μ is molecular mass, kg/kmol; λ is thermal conductivity, W/(m K); ρ is density, kg/m^3; τ is time, s; γ is dynamics viscosity, Pa s; w is velocity, m/s; θ is angle between the opposite direction of the normal to the surface and the incident beam, rad; φ is azimuthal angle, rad; χ_ω is spectral coefficient of absorption, m^{-1};. **Subscripts**: c is convective; f is phase change; g is gas; i is time index in a digital scheme; it is number of iteration; IT is number of final iteration of iterative cycle; I is index of control time; j is index of radial coordinate; J is index of droplet surface; co is condensation; l is liquid; m is mass average; tf is transit phase transformation regime; r is radiation; R is droplet surface; sr is radiation source; v is vapor; vg is vapor-gas mixture; ω is spectral; Σ is total; 0 is initial state; ∞ is far from a droplet; + is external side of a droplet surface; - is internal side of a droplet surface.

1 INTRODUCTION

Heat and mass transfer processes in liquid droplets are the basis for a number of energy and industrial technologies. Water dispersion is used for air conditioning, cooling of high temperature gases, processing of various surfaces and their protection against intensive thermal effects, the increase of gas turbine efficiency, and in plasma and laser technologies [1-3], etc. Understanding the thermal hydrodynamical processes of water droplets and their control is essential in order to optimize existing liquid dispersion technologies and to develop modern, more efficient ones. The issue here is that complex transfer processes in two-phase droplets and gas

flows happen under conditions of intensive interaction. The level of the interaction intensity is determined by a number of important factors, for example, the influence of the Stefan's hydrodynamic flow on the convective heating and evaporation of droplets, the influence of water droplet slipping in the flow on the external heat transfer and on the forced liquid circulation within the droplets, and the spectral nature of radiation. The optical spectral effects of light on the surface of droplets define the intensity of the radiation flow absorption in a semi-transparent liquid. Spectral radiation models [4-9], etc. allow the evaluation of the radiation input in the energy state of semi-transparent droplets. A proper knowledge of water spectral characteristics leads to a successful application of these models when defining radiation absorption in water droplets [10, 11]. In heat transfer and phase change thermal technologies, the variety of process conditions requires a systematic view in order to define the regularities of process interaction. For this purpose, the heat and mass transfer analysis of dispersed liquid droplets is a convenient tool in the cycle of consistently changing regimes of phase transitions. In the general case, the phase change cycle of water droplets dispersed in a wet gas flow will consist of condensation, transitional evaporation, and equilibrium evaporation regimes. Steam condensation occurs only when the temperature of the dispersed water is below the dew point. In the transitional evaporation regime, the droplets are heated to a thermal state that ensures equilibrium evaporation. When such a state is reached, all heat is then used for water evaporation. The equilibrium evaporation regime of a droplet plays an important role in technologies based on liquid evaporation, and thus has been thoroughly investigated [12]. The transitional evaporation regime of a droplet has been widely investigated in fuel dispersion technologies [13]. This study has numerically modeled the transitional phase change of water droplets in a wet gas flow in the case of complex heating by radiation and convection. The determination of droplet heat transfer boundary conditions helps to retain the aspects of water dispersion in a biofuel furnace and of the utilization of waste heat from the flue gas in a condensing shell and tube heat exchanger.

2 METHODOLOGY

Water dispersion can be used to regulate the biofuel combustion process in a furnace, to clean solid particles from the flue gas as well as to cool and wet it so that the process in a condensing shell and tube heat exchanger can be effective. In contact type condensing shell and tube heat exchangers, heat is recovered from the flue gas by condensing water vapor directly onto the dispersed water droplets. For such a technology, it is usually necessary to control the droplet heating to the dew point temperature and to use a transitional heat exchanger, the operation of which is usually burdened by condensate polluted with biofuel ash particles. In such types of condensing shell and tube heat exchangers, the vapor is condensed while the biofuel flue gas is flowing through the pipes, and thus the fluid flowing at the outside of the pipes receives heat through the wall. This technology requires optimal vapor condensation. Vapor condensation is a very complex process because of thermo-hydro-dynamical interaction processes between the polluted flue gas and the condensate's film. In order to improve those processes, water is dispersed additionally over the stack of the pipes. In these cases, consideration should be given to the heating of the dispersed water droplets and transitional phase change processes taking place at their surface. A complex analysis of droplet external and internal heat transfer and of phase change processes at the droplets' surfaces is necessary for the determination of the interaction between the dispersed water and the biofuel flue gas energy. R^+ and R^- radii relatively determine the external and internal surface of spherical droplets. In the case of complex heating, the total heat flux is determined by radiation and convective components, $q_\Sigma^+ = q_r^+ + q_c^+$ and $q_\Sigma^- = q_r^- + q_c^-$, respectively. In condensation $\tau \equiv 0$ to τ_{co}, transitional evaporation $\tau \equiv \tau_{co}$ to τ_e and equilibrium evaporation $\tau \equiv \tau_e$ to τ_f the relation of the heat fluxes at the surface of a droplet is:

$$\begin{aligned} q_\Sigma^-(\tau) &= q_\Sigma^+(\tau) + q_f^+(\tau), \text{ when } \tau \equiv 0 \text{ to } \tau_{co}, \\ q_\Sigma^-(\tau) &= q_\Sigma^+(\tau) - q_f^+(\tau), \text{ when } \tau \equiv \tau_{co} \text{ to } \tau_e, \\ q_\Sigma^-(\tau) &= q_f^+(\tau) - q_\Sigma^+(\tau), \text{ when } \tau \equiv \tau_e \text{ to } \tau_f. \end{aligned} \quad (1)$$

The magnitude of the total heat flux at the surface of the droplets is determined by the intensity of the complex external heating. The magnitude of the heat flux determines the energy intensity of the phase change at the droplet surface. The total heat flux at the droplet surface internal side determines the heating intensity

in the water droplets. In the condensation regime, the whole of the heat flux passed onto the droplet surface heats the water, while in the transitional evaporation regime it is only the part of the heat flux that is excluded from the evaporation process. In the equilibrium evaporation regime, the water is evaporated by the heat from the external heat transfer; the change in the enthalpy of cooling droplets may also take place in the process. Spectral light absorption indicators for water are finite [10]; therefore, it is assumed that water droplets do not absorb radiation through their surface and $q_r^- \approx q_r^+$. The external convective heat transfer flux of a droplet is described according to the model [14], where additionally the universal Spalding heat transfer B_T equation is adopted to phase change regimes according to the methodology in [15]:

$$q_c^+ = \left[\frac{\lambda_{vg}}{R} \frac{\ln(1+B_T)}{B_T} + \frac{\lambda_{vg}}{2R} \frac{0.552\,\mathrm{Re}^{1/2}\,\mathrm{Pr}^{1/3}}{(1+B_T)^{0.7}} \right](T_g - T_R), \quad B_T = \frac{c_{p,vg}(T_g - T_R)}{L}\left(1 + \frac{q_c^-}{q_c^+}\right). \tag{2}$$

In the case of the assumption of the diffusive layer surrounding an evaporating droplet being proportional to its radius $\delta(\tau) \equiv R(\tau)$, to describe the heat flux of phase change, the analytical model [16] for vapour flux is applied:

$$q_f^+ = m_v^+ L, \;\; m_v^+ = \frac{D_{vg}\mu_v}{T_{vg,R} R_\mu R} p \left[p_{v,R} - p_{v.\infty} + \frac{\mu_v}{\mu_{vg}} \left(\ln \frac{p - p_{v,\infty}}{p - p_{v.R}} - p_{v,R} + p_{v,\infty} \right) \right]. \tag{3}$$

The convective component of the total heat flux in a droplet is defined according to the modified Fourier's law:

$$q_c^-(\tau) = -\lambda_{l,ef}\, grad T_{r \equiv R^-}, \tag{4}$$

where the effective thermal conduction coefficient $\lambda_{l,ef} \equiv \lambda_l k_c^-$ s used to take into account the influence of water circulation on heat transfer within the droplet according to the methodology in [14]. In equation (4) the temperature gradient is defined by conduction and radiation in a semi-transparent spherical droplet for the case described by the transcendental system of differential and integral equations:

$$\rho_l c_p \frac{\partial T}{\partial \tau} = \frac{1}{r^2} \frac{\partial}{\partial r} \left(\lambda_l \frac{\partial T}{\partial r} - q_r \right), \tag{5}$$

$$q_r = \int_0^\infty \int_0^\pi \int_0^{2\pi} I_\omega \sin\Theta \cos\Theta d\Theta d\varphi d\omega, \;\; \frac{\partial I_\omega}{\partial s} = \chi_\omega \left[n_\omega^2 I_{\omega 0} - I_\omega \right], \;\; \chi_\omega = 4\pi k_\omega \omega, \;\; \bar{n}_\omega = n_\omega - i k_\omega. \tag{6}$$

The equation system (1-6) can be solved only using an iterative method, so that unambiguous conditions for the equations (5, 6) can be formulated with regard to the yet unknown functions of the droplet surface temperature and spectral radiation intensity at the internal surface of the droplet $I_{\omega R}(\tau)$:

$$R(\tau \equiv 0) = T_{l,0}; \;\; T_l(\tau \equiv 0) = T_{l,0}; \;\; T(r \equiv R^-, \tau) = T_R(\tau); \;\; I_\omega(r \equiv R^-, \tau) = I_{\omega,R^-}(\tau), \;\; \partial T(r \equiv 0, \tau)/\partial r = 0. \tag{7}$$

A combined analytical-numerical method is applied to solve the system (5-7). At first, the transfer cases (5) and (7) as well as (6) and (7) are analyzed analytically as independent cases. In the first case, the function of the local radiation flux $q_r(r,\tau)$ is assumed to be defined, and in the second case, the function describing the transient temperature field in a droplet $T(r,\tau)$ is assumed to be defined. Using the auxiliary function $\vartheta(r,\tau) = r[T(r,\tau) - T_R(\tau)]$, equations (5) and (7) are transformed into the Dirichlet heat transfer case with the defined source function [7] and the temperature field gradient in the expression (4) is described by an infinite line of integral equations:

$$\left.\frac{\partial T}{\partial r}\right|_{r \equiv R^-} = \frac{2\pi}{R^2} \sum_{n=1}^{\infty} n \int_o^\tau \left[\frac{R}{n\pi} \frac{dT_R}{d\tau} - \frac{1}{c_{p,l}\rho_l} \int_0^R q_r \cdot \left(\sin\frac{n\pi r}{R} - \frac{n\pi r}{R} \cos\frac{n\pi r}{R} \right) dr \right] exp\left[-a\left(\frac{n\pi}{R}\right)^2 (\tau - \tau_*) \right] d\tau_*. \tag{8}$$

In the case of the defined radial function $T(r)$ describing the temperature field in a droplet, the function of the local radiation flux $q_r(r)$ in equation (8) is calculated using the methodology of reference [6] that takes into account spectral light effects at both sides of the droplet surface, droplet radiation, and external source radiation, where the external source is assumed to be a black body with a biofuel flue gas temperature.

The dynamics of the droplet movement in the gas flow and the change in the droplets' mass and volume are defined by the following differential equations:

$$\frac{dw_l(\tau)}{d\tau}=\frac{3}{8}\frac{C_l(\tau)}{R(\tau)}\frac{\rho_g(\tau)}{\rho_l(\tau)}\frac{w_g(\tau)-w_l(\tau)}{\left[w_g(\tau)-w_l(\tau)\right]^{-1}},\qquad \frac{dM_l(\tau)}{d\tau}\equiv\frac{4\pi}{3}\frac{d\left[\rho_{l,m}(\tau)R^3(\tau)\right]}{d\tau}=\dot{m}_v=-4\pi R^2(\tau)m_v^+(\tau). \tag{9}$$

In respect of the time function $T_R(\tau)$ of the droplet surface temperature, the system of the algebraical and integral equations (1-4, 7-9) is solved numerically according to the iterative scheme using the fastest descending method. In order to form the numerical scheme, the non-dimensional coordinates for radius $\bar{r}=r/R(\tau)$ and time $\bar{\tau}=\tau/\tau_{co}$ are introduced (if there is no condensation regime, then $\bar{\tau}=\tau/\tau_{tf}$), that ensures the droplet radius equals 1 ($\bar{r}(R,\tau)=1$), and the duration of the first phase change regime is also 1 ($\bar{\tau}(\tau=\tau_{co})=1$). Then variational steps of the radial and time coordinates are defined as:

$$\Delta\bar{\tau}=\frac{1}{I-1},\quad \Delta\bar{r}=\frac{1}{J-1},\quad \sum_{i=2}^{I}\left(\bar{t}_i-\bar{t}_{i-1}\right)=1,\quad \sum_{j=2}^{J}\left(\bar{r}_j-\bar{r}_{j-1}\right)=1. \tag{10}$$

For every time step starting with the second one $\tau_i=\tau_{i-1}+\Delta\bar{\tau}\cdot\tau_{co}$, the descent fastest methods in iterative $it\equiv 1$ to IT cycle proceeds to define the instantaneous temperature $T_{R,i}\equiv T_{R,i,IT}$ of the droplet surface. The droplet surface temperature $T_{R,i,it=IT}$ attributed to the final iteration IT must ensure that the calculated heat fluxes would fulfill the condition of the expression (1) with a maximum error of five hundredths of a percent:

$$\left|1-\frac{q_{c,i,IT}^-}{q_{c,i,IT}^+\pm q_{f,i,IT}^+}\right|\times 100\,\%\le\delta=0.05\,\%. \tag{11}$$

The droplet heat and mass transfer parameters $R_{i,it}$, $q_{c,it}^+$, $q_{c,it}^-$ and $T_{i,j,it}$ that are necessary for an it iteration, however, are not yet defined; they are used from $it-1$ iteration calculated parameters $P_{i,it}\equiv P_{i,it-1}$. Later the $P_{i,it}$ parameters are revised. The mesh $I=21,\ J=41$ is used in the numerical modeling; the radiation spectrum is gradually divided into $M-1=100$ parts according to the wave number $\omega\equiv 10^3$ to $1.25\cdot 10^6$. In equation (8) the number N of the line terms is defined in an infinite sum ($\sum_{n=1}^{\infty}\cdot$) i. e., it is assumed that $\infty\equiv N$ when N=121. For the defined surface temperature $T_{R,i,IT}$, all the necessary instantaneous P_i parameters of the droplet heat and mass transfer are calculated.

3 RESULTS

The biofuel flue gas is defined by the velocity w_g, the temperature T_g and humidity of $\bar{p}_v\equiv p_v/p$, where $p=0.1$ MPa. The dispersion of the water of temperature T_l is defined by the dispersion of droplets of diameter $2R$ and initial velocity w_l. The relative water flow rate is assumed to be $G_l/G_g\to 0$ and therefore the influence of water droplets on air parameters is not taken into account. The droplet heating process is defined by the Reynolds number $\mathrm{Re}=2R\rho_g\left|w_l-w_g\right|/\gamma_{vg}$. The existence of the radiation source is defined by parameter $\bar{T}_{sr}\equiv T_{sr}/T_g$: $\bar{T}_{sr}=0$ in the case of convective heating, and $\bar{T}_{sr}=1$ in the case of complex heating.

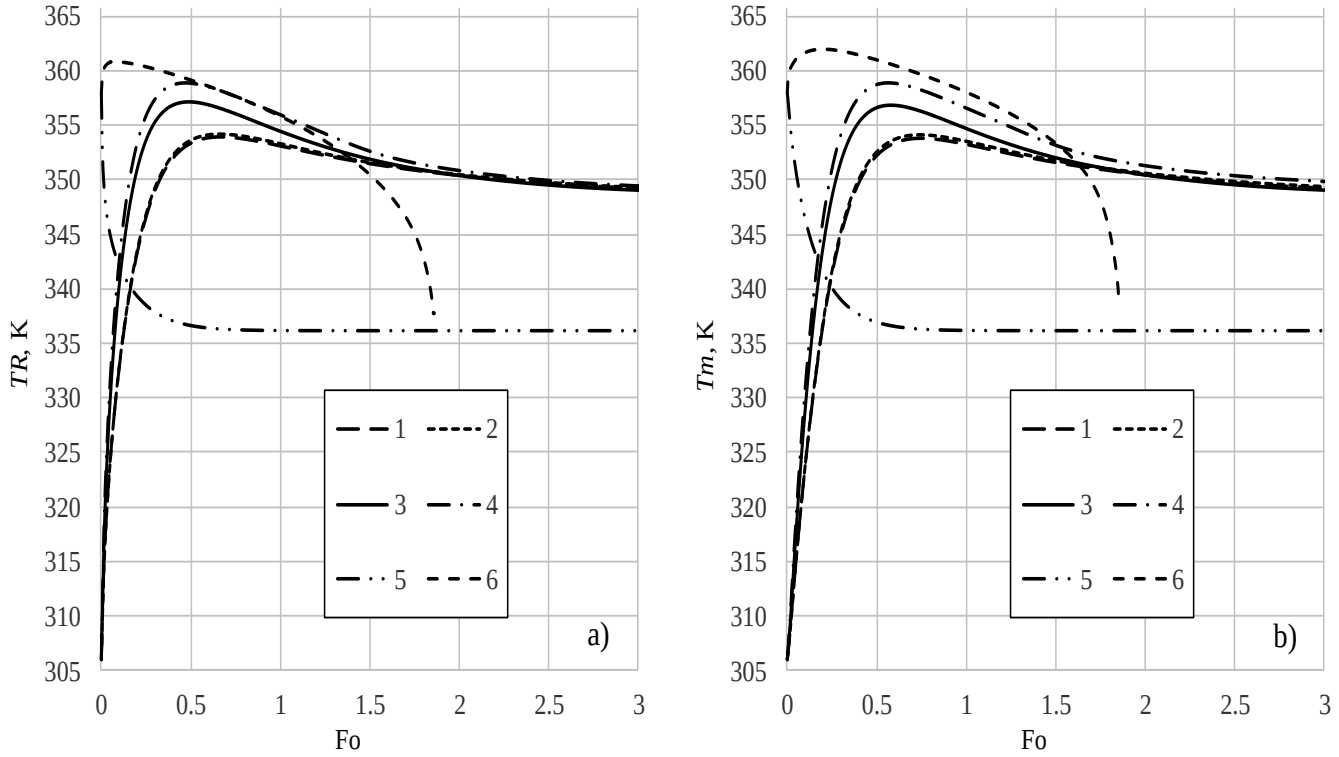

Fig. 1. The influence of water droplet dispersity and heating process on the variation of their surface temperature (a) and average mass temperature (b). $R_0 \times 10^6$, m: (1, 2) 50, (3, 4) 100, (5, 6) 1500; $\overline{T}_{sr}$: (1, 3, 5) 0, (2, 4, 6) 1; Re_0: (1, 2) 49.4, (3, 4) 246.98, (5, 6) 0; $T_{l,0}$, K: (1-4) 306, (5, 6) 358; $w_{l,0}$, m/s: (1-4) 65, (5, 6) 0; w_g, m/s: (1-4) 15, (5, 6) 0; $T_g = 1133\,\mathrm{K}$; $\overline{p}_v$: (1-6) 0.2, (7, 8) 0; a_0 / R_0^2: (1, 2) 53.572, (3, 4) 2.14288, (5, 6) 0.059524.

The results have been analyzed in the time scale of the Fourier number $\mathrm{Fo} = \left(a / R_0^2\right) \cdot \tau$ where the individual multiplier $a\left(T_l \equiv 278\,\mathrm{K}\right) / R_0^2$ ensures a more convenient graphical $P(\mathrm{Fo})$ analysis of time functions $P(\tau)$ for droplets of different sizes [15]. The time function of the droplet surface temperature $T_R(\tau)$ and the time function of the average mass temperature $T_m(\tau)$ are important when describing the variation in thermal condition of the heated droplet. These temperatures are sensitive to the temperature of the dispersed water and the droplet heating process (Fig. 1). Figure 1 presents the change in the thermal state of water droplets for different droplet heating processes: curves 1 and 3 represent convective heating, curve 5 conductive heating, curves 2 and 4 complex heating convection plus radiation, and curve 6 complex heating conduction plus radiation. It is convenient to describe the thermal state of dispersed water using the relation ($\overline{T}_{l,0} \equiv T_{l,0} / T_{l,e}$) between the temperatures of dispersed water $T_{l,0}$ and equilibrium evaporation of droplets $T_{l,e}$. It is assumed that in the equilibrium evaporation regime the heat provided to the droplets serves to evaporate the water. At the initial state of phase change, the droplets of cold water of temperature 306 K warm up (Fig. 1, curves 1–4 and 6), and the droplets of warm water of 358 K temperature cool down (Fig. 1 curve 5). It is necessary to note that the droplets with an initial temperature of 358 K during the complex heating within a dry air flow of 1313 K are described as cold water, but in the case of conductive heating they represent warm water. In the flow of humid air, at the surface of cold water droplets, which are warming up, water vapour condenses until the surfaces warm up to the dew point temperature at the time $\tau \equiv \tau_{co}$ (Fig. 1 a). For the humid air case modeled, the dew point temperature was 333.53 K. At the moment of the change to the evaporation regime, the temperature of the droplet's central layers is lower than the dew point temperature.

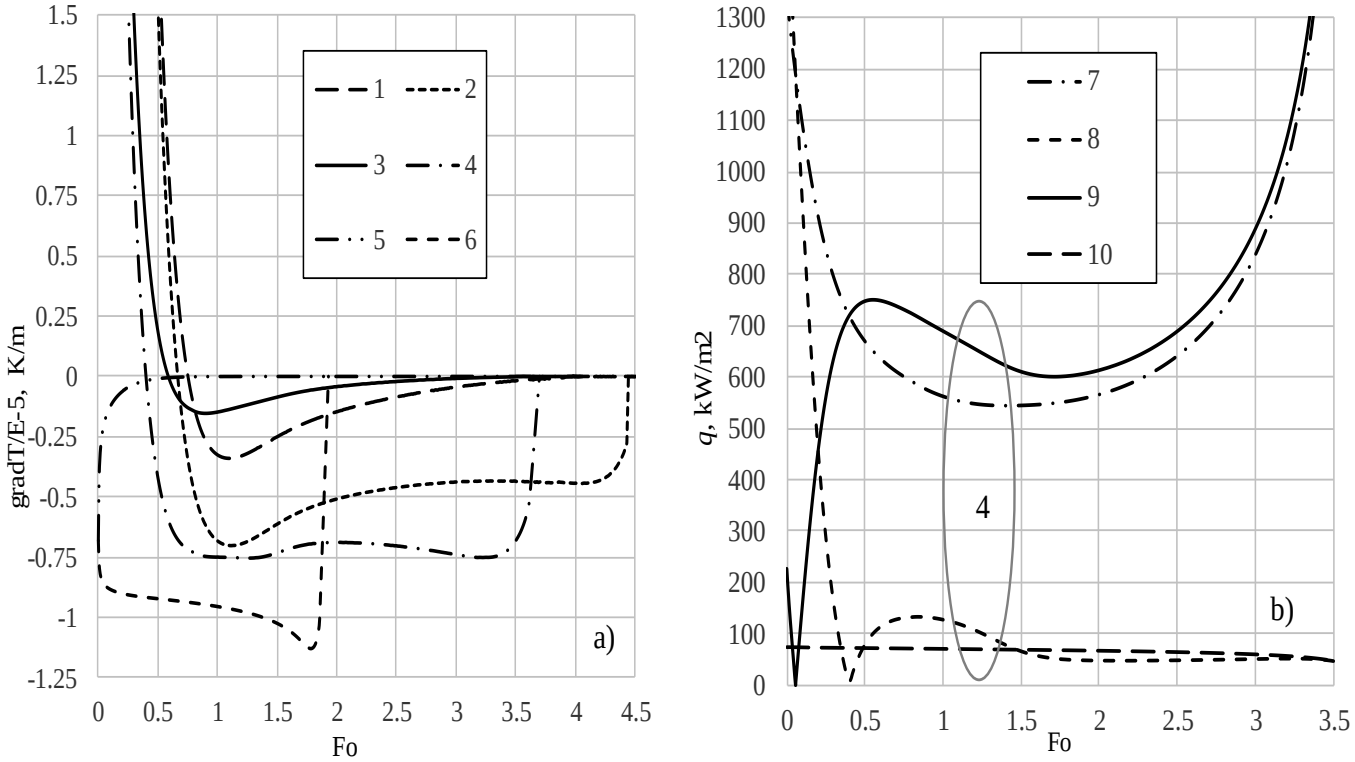

Fig. 2. The influence of the heating process for (a) the dynamics in the temperature field gradient in droplets and (b) the variation of heat fluxes at a droplet's surface in the case of complex heating. Parameter q: (7) $q_{c,g}$, (8) $q_{c,l}$, (9) q_f, (10) q_r. Other symbols as in Fig. 1.

The droplets of hot water evaporate in the equilibrium regime and cool down, while the droplets of cold water warm up to the equilibrium evaporation thermal state, expressed by the temperature $T_{l,e}$, in the transitional evaporation regime. When trying to define the onset of the equilibrium evaporation regime of cold water droplets, their warming up process must be considered. In the case of convective heating, the surfaces of droplets warm up to the highest temperature. In the case of a complex heating process, the central layers of the droplets reach the highest temperature as a result of thermal effects from absorbed radiation. The droplets cool down in the equilibrium evaporation regime (Fig. 1). The characteristics of the variation in the droplets' thermal state are clearly displayed in the dynamics of the temperature gradient in the droplets (Fig. 2 a). The start of the equilibrium evaporation of the cold water droplets being heated by convection is defined by their surface warming to the highest temperature $T_{l,e,c} \equiv T_R(\tau_e) = T_{R,max}$ and in the case of complex heating, it is their mass warming up to the highest temperature $T_{l,e,cr} \equiv T_m(\tau_e) = T_{m,max}$. The dynamics of the average temperature of the droplet mass is described by the following function of the transient temperature field $T(r, \tau)$:

$$T_m(\tau) = \int_0^{R(\tau)} \rho_l(r,\tau) T(r,\tau) r^3 dr \Big/ \int_0^{R(\tau)} \rho_l(r,\tau) r^3 dr \tag{12}$$

For the modelled warm up of cold water droplets in air of 1133 K temperature, the calculated duration τ_e of the transitional phase change ($\tau \equiv 0$ to τ_e) regime for the boundary conditions defined for assumptions (1–4 and 6) presented in Fig. 1 is 0.0031, 0.00346, 0.037, 0.0423 and 3.36, respectively. The calculated temperature $T_{l,e}$ for the onset of the equilibrium evaporation regime is 353.96, 354.15, 357.17, 358.92 and 362.01 K, respectively. In the case of complex heating, in the transitional phase change regime, the temperature gradient in a droplet changes direction when crossing the zero value and then reaches the maximum value (Fig. 2 a, curves 2, 4 and 6). However, in the case of convective heating, the temperature gradient in a droplet reaches the zero value consistently in the transitional phase change regime and changes in direction only when the droplet starts to cool down in the equilibrium evaporation regime (Fig. 2 a, curves 1, 3). At the initial stage of equilibrium evaporation, the temperature gradient of a droplet that is heated using

conductivity consistently approaches the zero value and then the zero value remains (Fig. 2 a, curve 5); thus, the droplet of 358 K temperature cools down to the calculated temperature 336.17 K, and remains at the same thermal state (Fig. 1, curve 5).

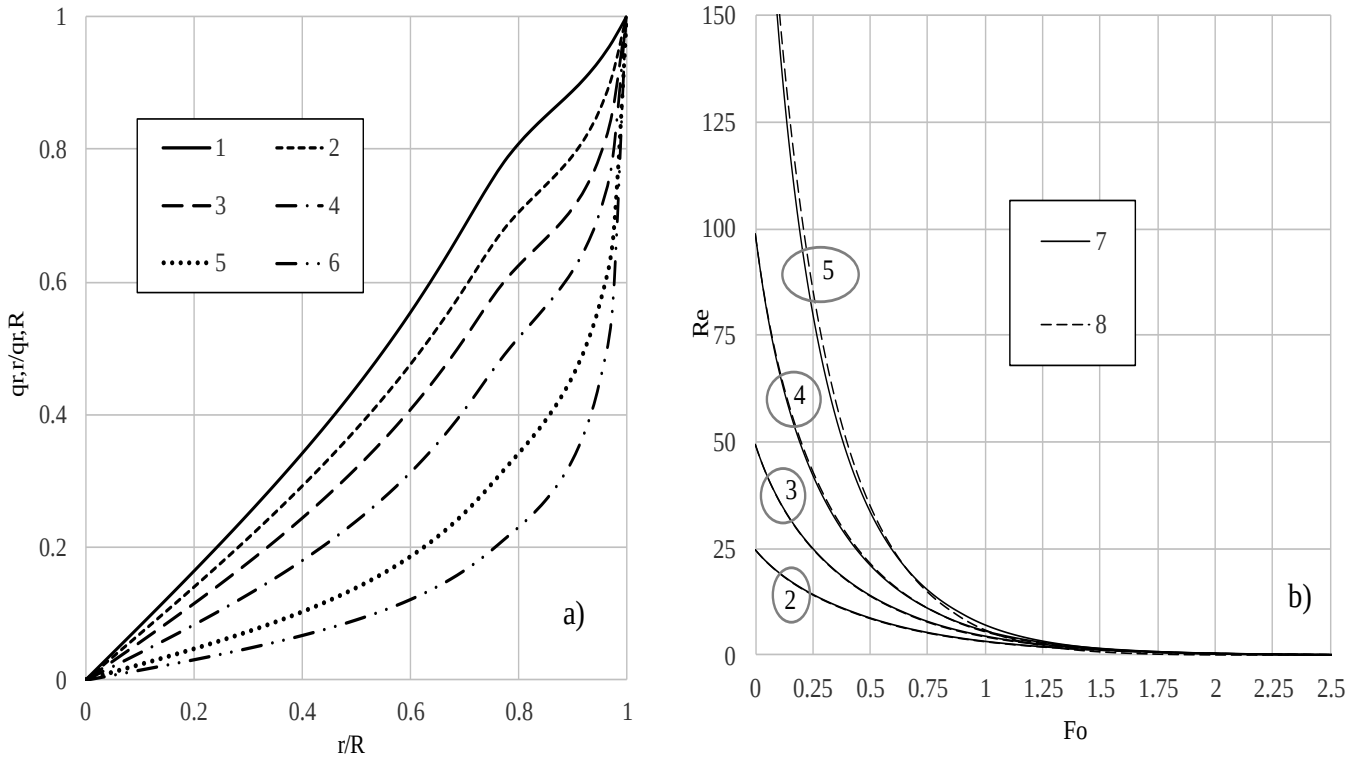

Fig. 3. Local radiation flux in droplets (a) and the variation of the Reynolds number (b). $\overline{T}_{sr}$: (7) 0, (8) 1; $R_0 \times 10^6$, m: (1) 10, (2) 25, (3) 50, (4) 100, (5) 250, (6) 500; $q_{r,R}$, kW/m^2: (1) 39.77, (2) 53.78, (3) 63.64, (4) 71.31, (5) 77.93, (6) 81.19; $T_{l,0}$, K: (a) 306, (b) 358; $w_{l,0} = 65$ m/s; $T_g = 1133$ K; $w_g = 15$ m/s; $\overline{p}_v = 0.2$.

The specific features of the variation in energy state of cold water droplets in humid air are clearly displayed in the Fig. 2 b diagram for heat flux variation at the surface of a droplet of 200 μm diameter. In the condensation regime, the initial energy impulse to the droplets is very strong and is defined by the sum of the calculated of initial convective (1348.56 kW/m^2) and condensation (227.11 kW/m^2) heat flux. In the process of the condensation regime, the condensation heat flux drops to zero. Hence, the convective heat flux to a droplet and the convective heat flux within the droplet become equal at the moment τ_{co} of phase change from condensation to evaporation regime, and the calculated heat flux in this case is 1192.09 kW/m^2 (Fig. 2 b, the intersection of curves 7 and 8). Two characteristic periods can be distinguished when analyzing the specific features of the convective heat flux $q_{c,l}$ variation in the transitional phase change regime. In the first period, $q_{c,l}$ consistently reaches a zero value, while in the second period it increases and equals the value $q_{r,e}$=69.4 kW/m^2 of the absorbed radiation flux in the droplet at the moment τ_e (Fig. 2 b, the second intersection of curves 8 and 10). At the end of the first period, the temperature gradient in a droplet reaches a zero value (Fig. 2 a, curves 2 and 4) and it changes in direction. The temperature field of the negative gradient forms conditions for the radiation heat absorbed in the droplet to flow to the surface of the droplet by internal convection and to participate in the process of water surface evaporation. At the end of the second period, the temperature gradient in the droplet ensures the full extraction of the absorbed radiation flux to the droplet's surface and participation in the water evaporation process. Hence, the calculated $q_{c,l}$ and q_r at the moment τ_e are equal and $q_f(\tau = \tau_e) = q_{c,g,e} + q_{c,l,e} \equiv q_{c,g,e} + q_{r,e}$. At the beginning of the equilibrium evaporation, the increase of $q_{c,l}$ is defined by the cooling droplet enthalpy. Later, when the cooling of the droplet decreases asymptotically (Fig.

1, curve 4), $q_{c,l}$ starts to decrease also, and the specific features of radiation flux absorption in the droplet, diminishing due to evaporation, become more relevant to its further dynamics $q_{c,l}(Fo>1)$ (Fig. 3 a). Thus, the factors relevant to the droplet energy variation are the process of radiation absorption in semi-transparent droplets and droplet slipping dynamics in the air flux. The droplet slipping dynamics have influence on the Reynolds number variation that defines the intensity of the external convective heating (Fig. 3 b). A droplet slipping quickly diminishes in the transitional phase change regime due to resistance forces, and radiation has no significant influence on that (Fig. 3 b). Hence, the intensities $q_{c,g,c}$ and $q_{c,g,cr}$ of the convective heat fluxes for the droplets with the same diameter are similar in the transitional phase change regime, while in the case of complex heating at the end stage of equilibrium evaporation, $q_{c,g,cr}$ starts to increase faster (Fig. 4 a) due to the quicker diminishing of more intensively evaporating droplets (Fig. 5 a).

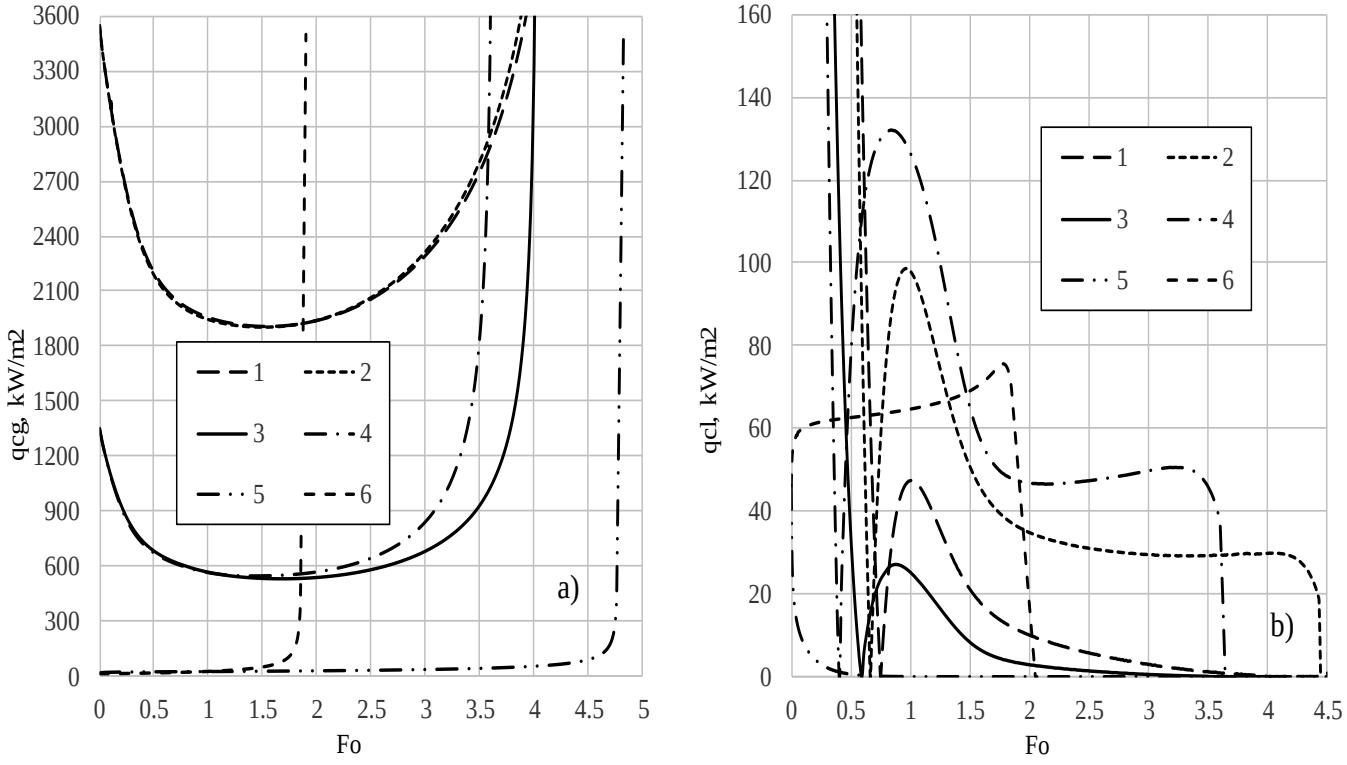

Fig. 4. The dynamics of the convective heat flux to the droplets (a) and within the droplets (b). $q_{c,g,0}$, kW/m^2: (1, 2) 3548.05, (3, 4) 1348.56, (5, 6) 13.758; $q_{f,0}$, kW/m^2: (1, 2) 908.44, (3, 4) 227.11, (5, 6) 59.994; $q_{c,l,0}$, kW/m^2: (1, 2) 4456.49, (3, 4) 1575.67, (5, 6) 46.236; $q_{r,0}$, kW/m^2: (1, 3, 5) 0, (2) 53.78, (4) 71.31, (6) 84.13. Symbols are the same as in Fig. 1.

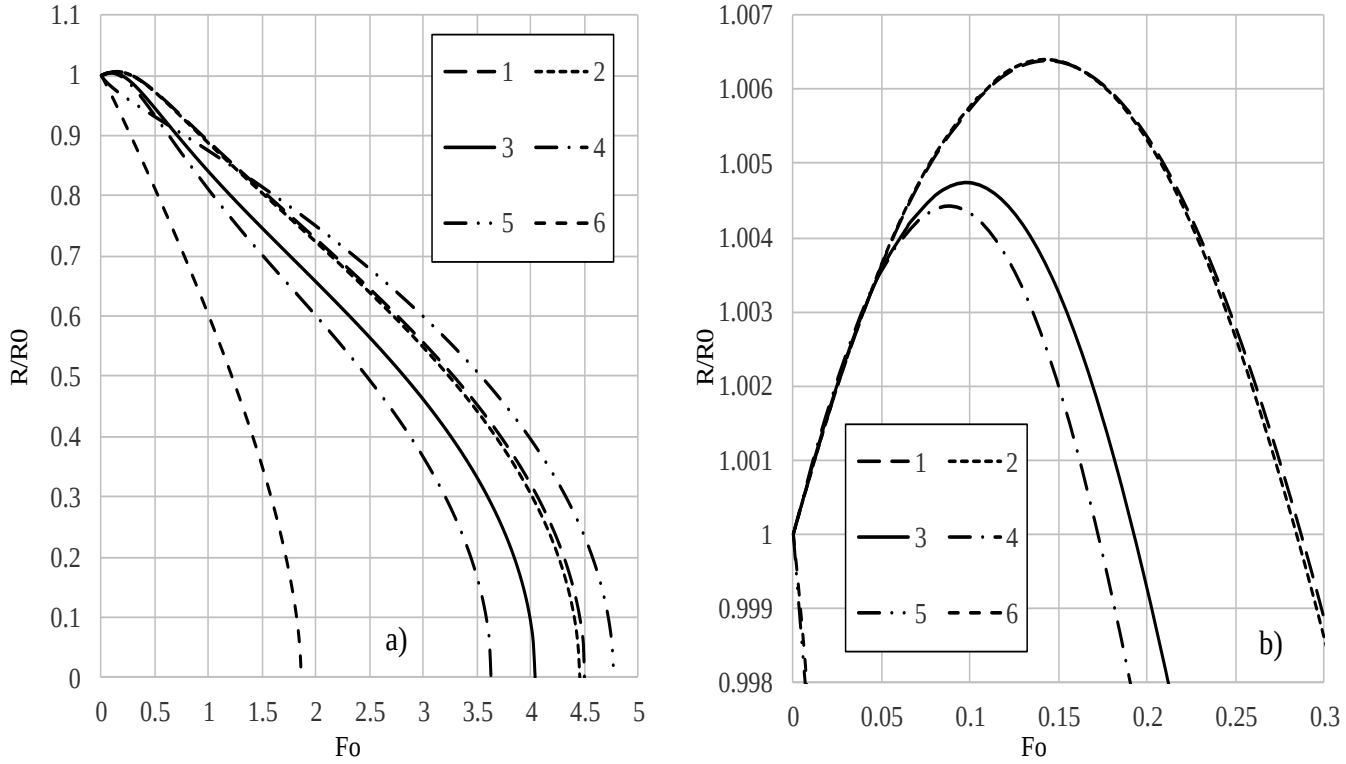

Fig. 5. The dynamics of droplet relative diameter R/R_0 in the phase change cycle (a) and in the process of transitional phase change (b). R_{max}/R_0: (1) 1.00636, (2) 1.00641, (3) 1.00474, (4) 1.00443, (5, 6) 1. Symbols are the same as in Fig. 1.

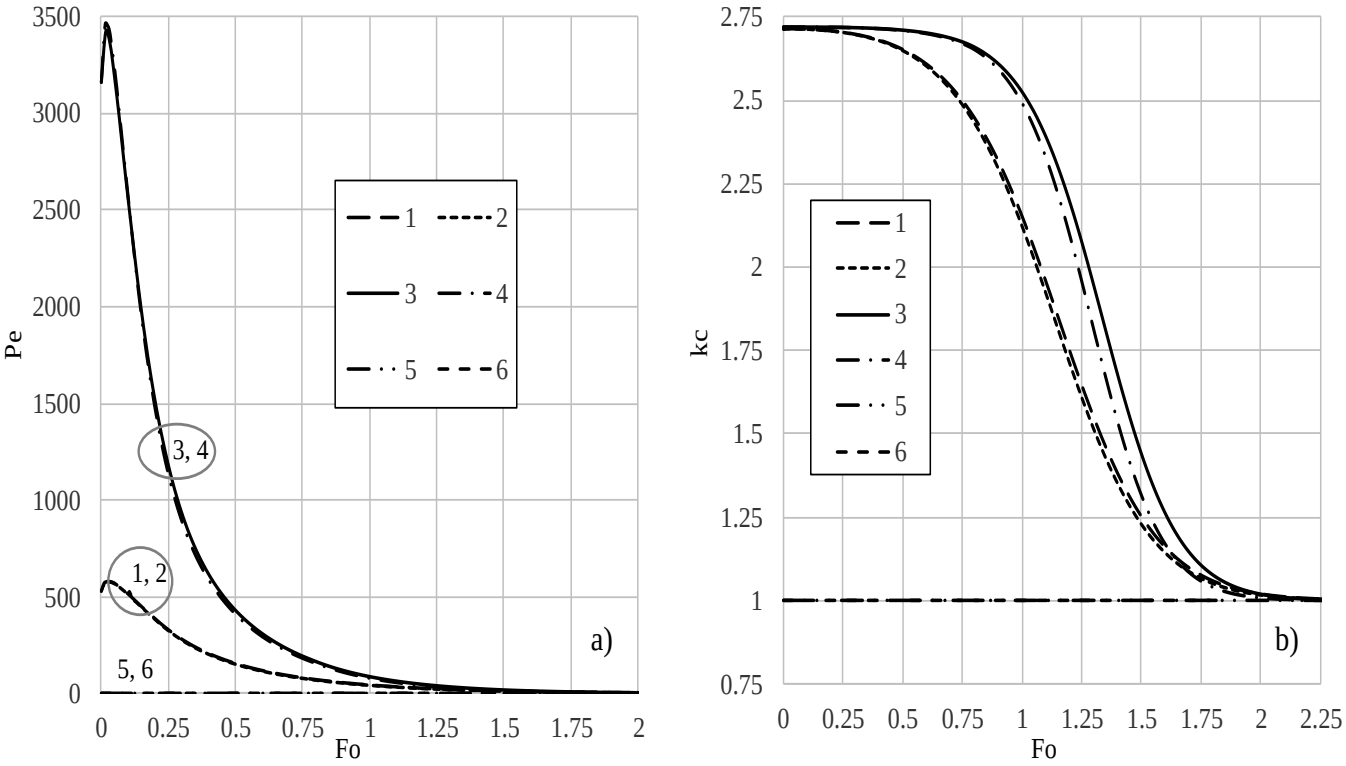

Fig. 6. Droplet slipping influence on the Peclet number (a) and on effective thermal conductivity parameter (b). Symbols are the same as in Fig. 1.

At the initial stage of the transitional phase change regime in an air flow, the droplets of cold water of temperature 306 K increase in size while the warming water is expanding, and while water vapor is condensing on their surfaces (Fig. 5 b, curves 1–4). At the beginning of transitional evaporation, the water expansion effect is still stronger than the diminishing effect of the evaporating droplet. The dimensions of the droplet are the largest at the moment these effects become equal. In dry air of high temperature, droplets start to diminish

immediately (Fig. 5, curves 5, 6). In the case of complex heating, the variation of the thermal state of the central layers of the droplets (Fig. 2 a) is determined by the processes of water circulation and radiation absorption. Water circulation is defined by the friction forces at the surfaces of slipping droplets. Their intensity is assessed based on the Peclet number (Fig. 6 a), which describes the effective thermal conductivity parameter (Fig. 6 b), which is an expression of the dominance of convection within a droplet compared to thermal conductivity. As the droplet slipping diminishes, the convective thermal transfer becomes weaker and $k_c(\mathrm{Fo} > 2) \approx 1$ (Fig. 6 b). For this reason, the heat within droplets is transferred via conductivity from Fo > 2 and via conductivity and radiation in the case of complex heat transfer. The distribution of local radiation flux in droplets is non-linear and depends heavily on droplet dispersity (Fig. 3 a). The most intensive absorption of radiation in large droplets occurs on the surface layers. As the droplets diminish through the evaporation process, a stronger influence is from non-linear spectral optical effects on the surfaces of the droplets, and the radiation absorption process changes under their influence (Fig. 3, curves 1–4). Essential changes in the intensity of radiation absorption are observed at the last stage of the equilibrium evaporation regime when the droplets are diminishing in size quickly. The qualitative change in the process of radiation flux absorption is clearly displayed in the dynamics of convective heat flux in the droplet in the second part of the equilibrium evaporation regime (Fig. 2 b, curve 8). In order to define the influence of radiation absorption effects, more extensive and detailed research is necessary within the range of wide boundary conditions.

In the utilization process of the thermal energy of biofuel flue gas, the temperature of the flue gas decreases monotonically to the temperature of the flue gas exhausted to the atmosphere. As the temperature of the flue gas decreases, the role of radiation becomes less significant for the condition of complex transfer processes. To highlight the tendencies, a cycle of the phase change has been modeled in water droplets dispersed into the air flow of the intermediate temperature 678 K between the temperatures of a furnace and the biofuel flue gas exhaust. In the case of conventional technologies, the humidity of cooling flue gas does not change; therefore, the average humidity of $\bar{p}_v = 0.2$ normal to the flue gas of a biofuel furnace has been preserved. In the flue gas of a lower temperature, the droplets start the equilibrium evaporation at a lower temperature (Fig. 7), but the influence of the transitional phase change condensation regime increases (Fig. 8).

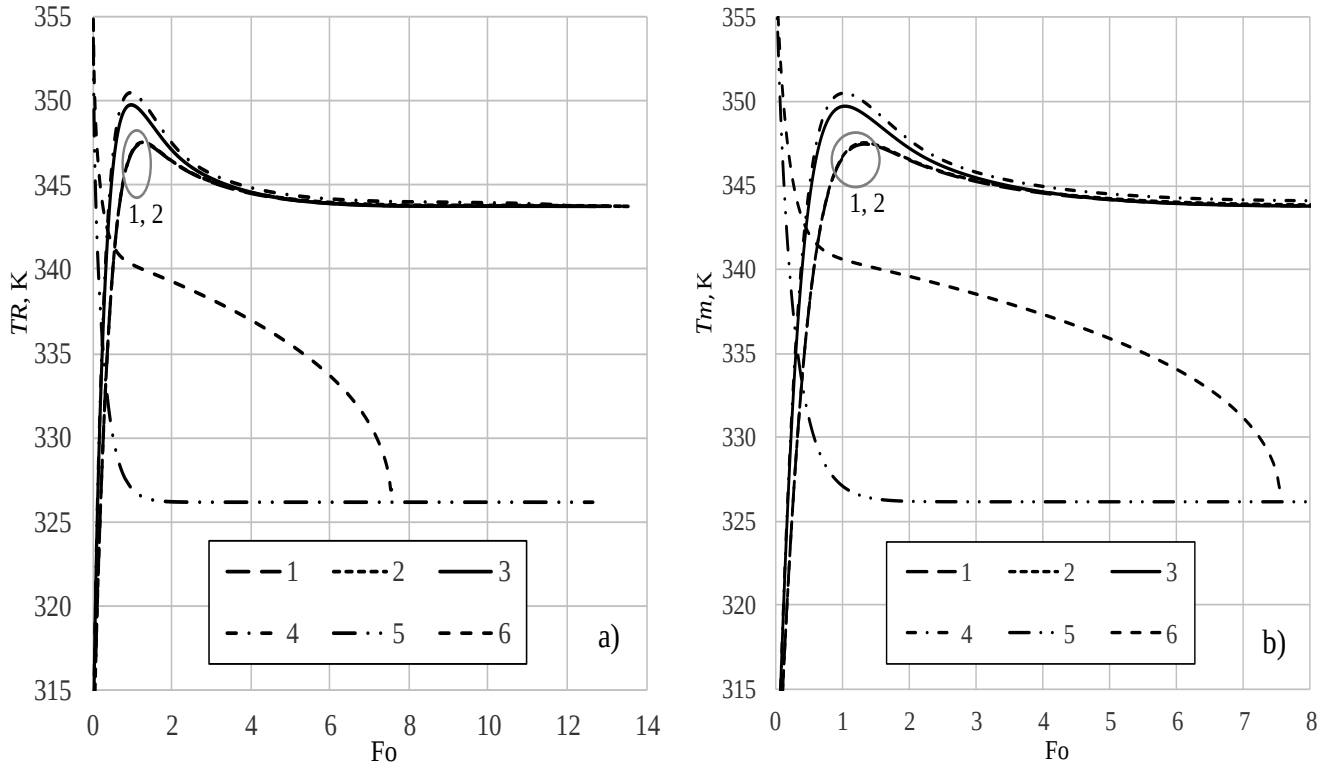

Fig. 7. The influence of the dispersity and heating process on the variation of the surface temperature of water droplets (a) and the variation of mass average temperature (b) in the air flow of 678 K temperature. $R_0 \times 10^6$, m: (1, 2) 50, (3, 4) 100, (5, 6) 1600; $\bar{T}_{sr}$: (1, 3, 5) 0, (2, 4, 6) 1; Re_0: (1, 2) 49.4, (3, 4) 246.98, (5,

6) 0; $T_{l,0}$, K: (1-4) 306, (5, 6) 358; $w_{l,0}$, m/s: (1-4) 65, (5, 6) 0; w_g, m/s: (1-4) 15, (5, 6) 0; $T_g = 1133$ K; $\bar{p}_v$: (1-6) 0.2, (7, 8) 0; a_0 / R_0^2: (1, 2) 53.572, (3, 4) 2.14288, (5, 6) 0.052316.

In the dry air flow of 678 K temperature, the droplets of 358 K temperature satisfy the warm water condition $\bar{T}_{l,0} < 1$, irrespective of their heating process. In the case of conductive heating, the droplets cool down to 326.14 K temperature (Fig. 7, curve 5) at the initial evaporation stage, while in the case of complex heating, the droplets approach this temperature at the final evaporation stage (Fig. 7, curve 6). In the humid air flow of temperature 678 K, the droplets of 306 K temperature satisfy the cold water condition $\bar{T}_{l,0} > 1$ and, in the transitional phase change regime, warm up to the highest equilibrium evaporation temperature 347.5, 347.55, 349.79 and 350.5 K calculated for the boundary conditions (1–4), respectively, defined in Fig. 7.

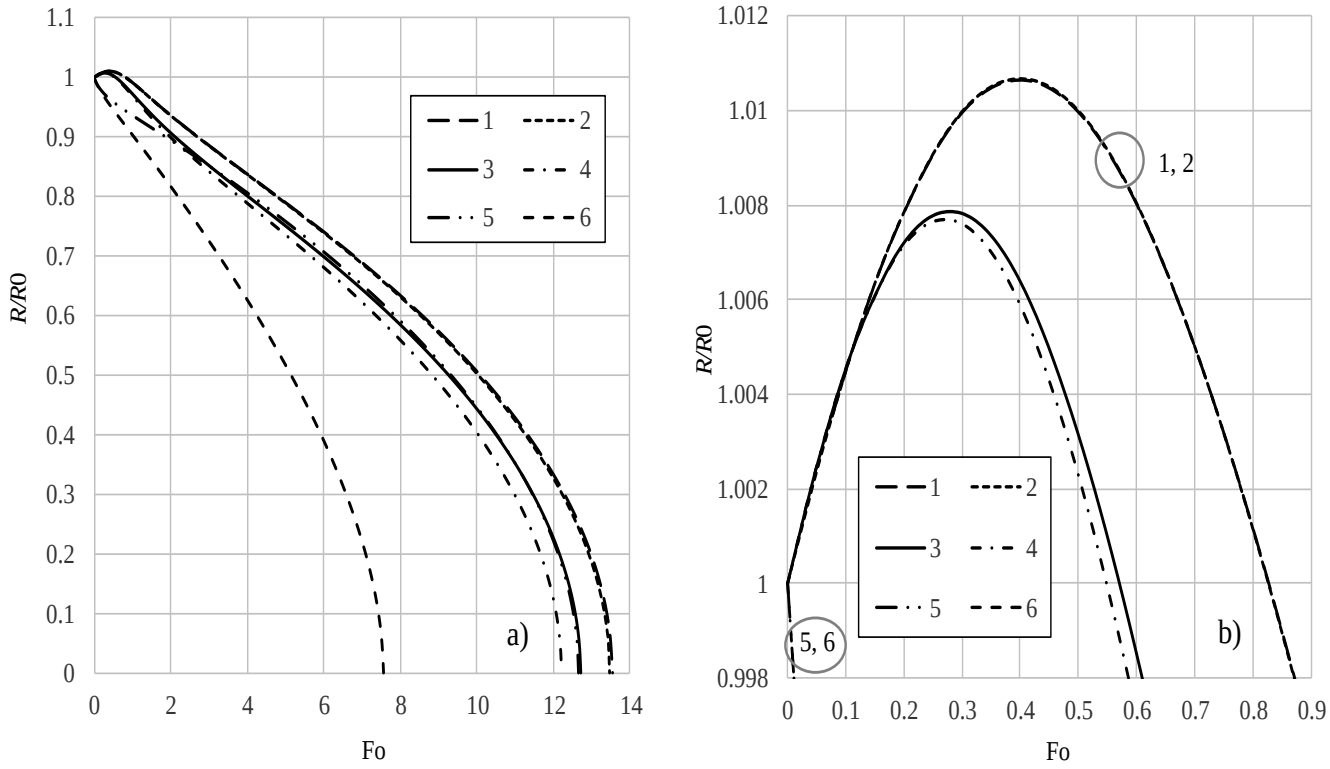

Fig. 8. The dynamics of the relative R/R_0 diameter of the water droplets warming up in the 678 K air flow in the phase change cycle (a) and in the process of transitional phase change (b). R_{max}/R_0: (1) 1.00636, (2) 1.00641, (3) 1.00474, (4) 1.00443, (5, 6) 1. Symbols are the same as in Fig. 7.

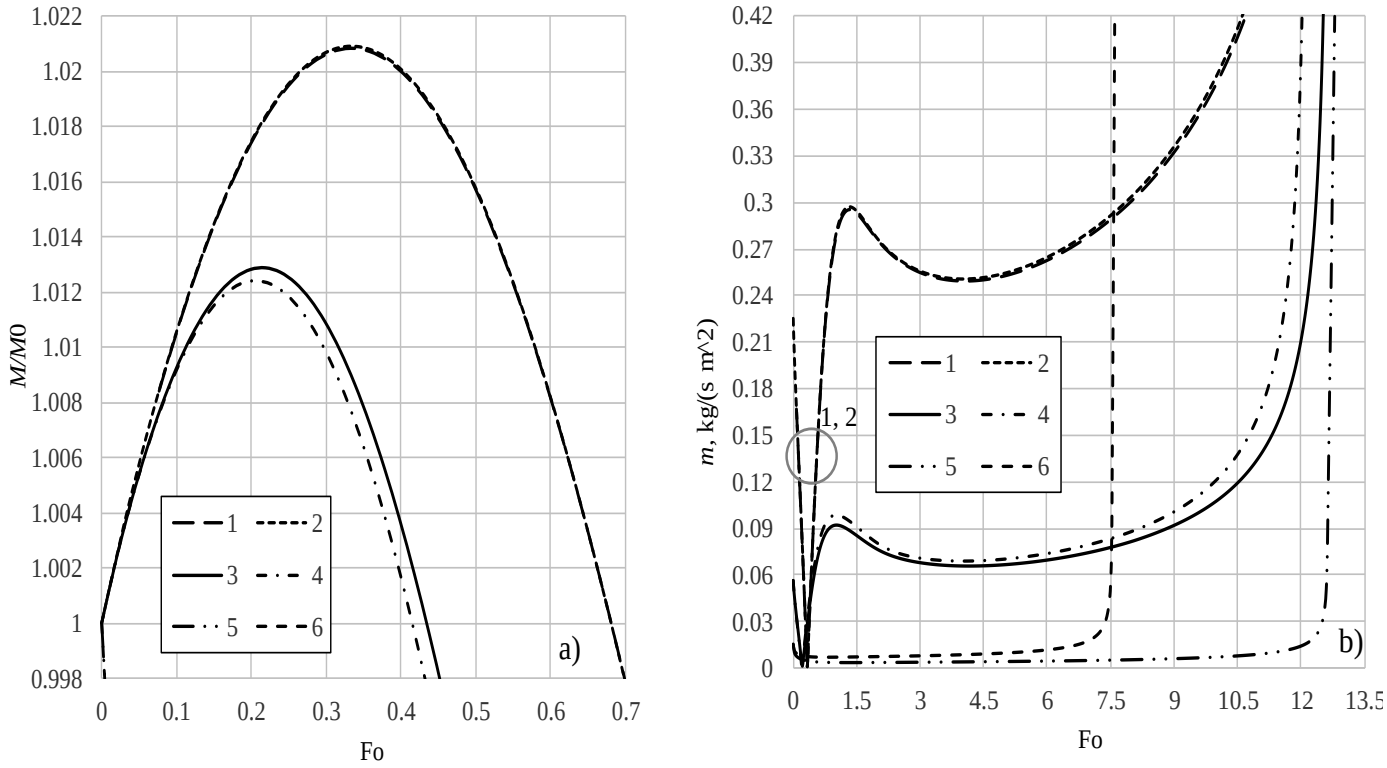

Fig. 9. The variation of the relative M/M_0 mass of the water droplets warming up in the 678 K air flow in the transitional phase change regime (a) and the variation of vapor mass flux in the phase change cycle (b) in the process of transitional phase change. M_{max}/M_0: (1) 1.02085, (2) 1.02093, (3) 1.01289, (4) 1.01242, (5, 6) 1; $m_{v,0}$, kg/(m^{2}s) : (1, 2) 0.2253, (3. 4) 0.05633, (5, 6) 0.01522. Symbols are the same as in Fig 7.

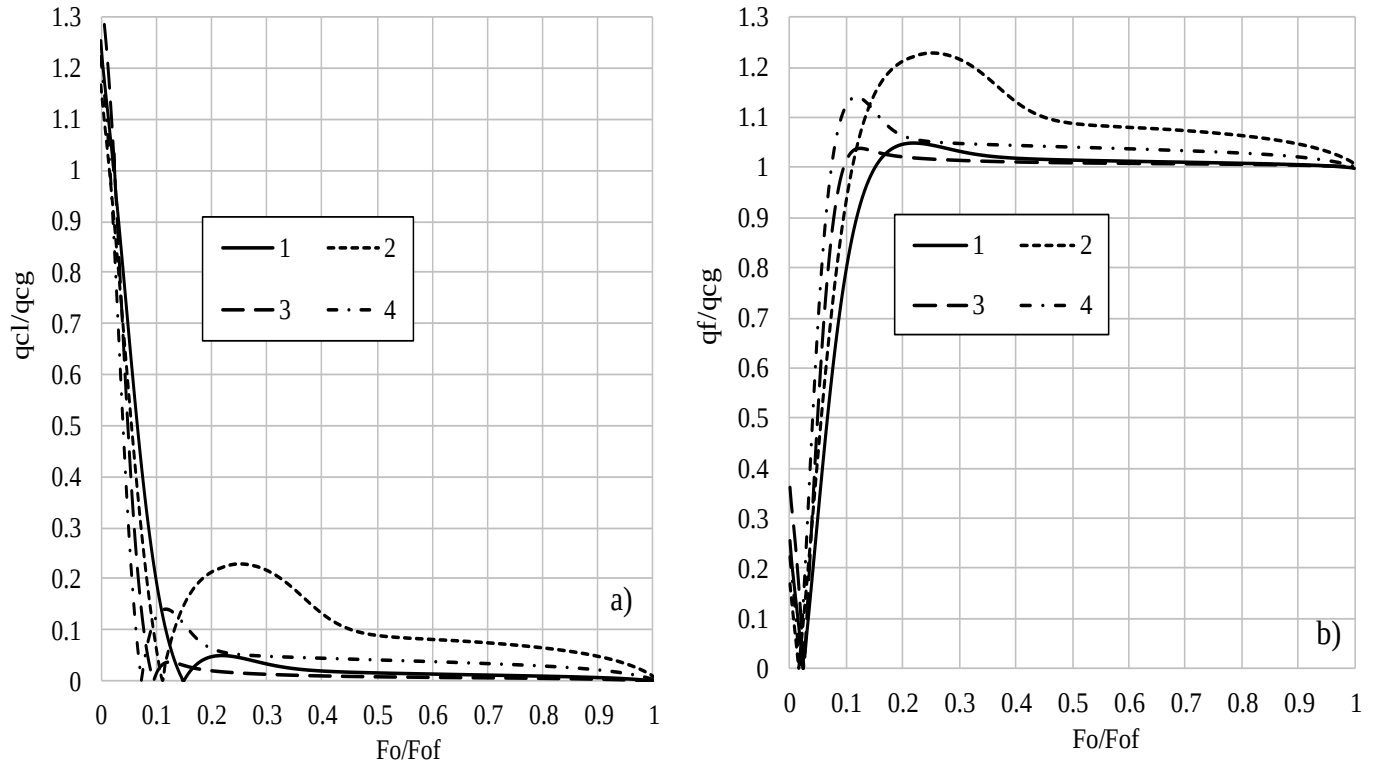

Fig. 10 The variation of heat flux ratio q_{cl}/q_{cg} (a) and ratio q_f/q_{cg} (b) in the process of water droplet phase change in the case of complex heating. $R_0 \times 10^6$, m: (1, 3) 25, (2, 4) 100; T_g, K (1, 2) 1133, (3, 4) 678; $T_{l,0} = 306$ K ; $w_{l,0} = 65$ m/s ; $w_g = 15$ m/s ; $\bar{p}_v = 0.2$.

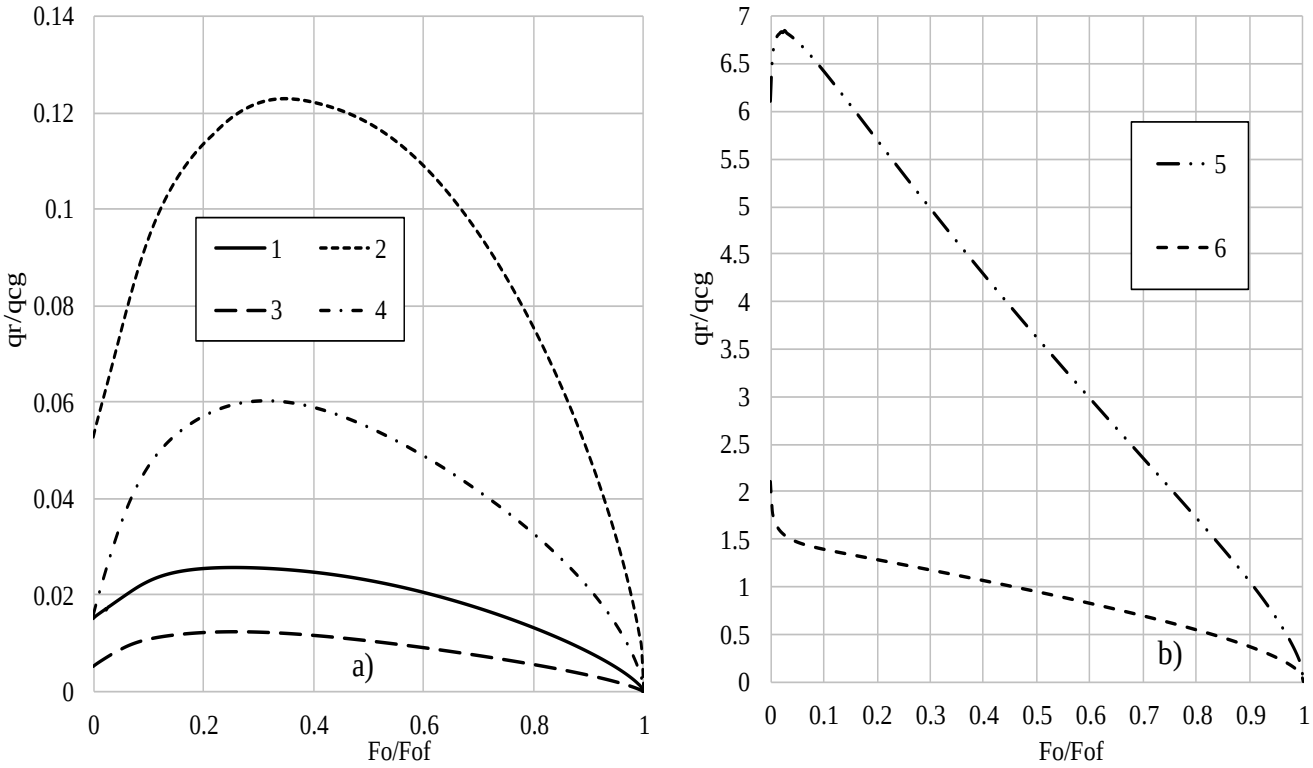

Fig. 11. The variation of heat flux ratio q_r/q_{cg} in the process of water droplet phase change in the case of complex heating. $R_0 \times 10^6$, m: (1, 3) 25, (2, 4) 100, (5) 1500, (6) 1600; T_g, K (1, 2, 5) 1133, (3, 4, 6) 678; $T_{l,0}$, K: (1-4) 306, (5, 6) 358; $w_{l,0}$, m/s: (1-4) 65, (5, 6) 0; w_g, m/s: (1-4) 15, (5, 6) 0; $\bar{p}_v = 0.2$.

The calculated durations τ_e of the transitional phase transition regime $\tau \equiv 0$ to τ_e for cases (1–4) are 0.00598, 0.00621, 0.0729 and 0.077 s, respectively, and the calculated duration τ_{co} of the condensation regime in it is quite clear and is 0.00156, 0.00156, 0.016 and 0.0154 s, respectively. For the cases modeled, the radii of cold water droplets increased to 25.266, 25.267, 100.787 and 100.77 μm respectively, in the condensation regime and at the beginning of the equilibrium evaporation. Therefore, the radii of small droplets increased by more than 1 percent (Fig. 8 b), and their mass increases by more than 2 percent in the condensation regime (Fig. 9 a).

The variation of the water droplets' thermal and energy state is defined by the heat flux dynamics on the droplet's surface. In order to describe the specificity of the dynamics mentioned, the dynamics of non-dimensional heat fluxes q_{cg}/q_n q_r/q_n, q_{cl}/q_n, and q_f/q_n expressed via the heat flux ratio $\bar{q} \equiv q/q_n$ is important. When choosing a normalizing heat flux q_n, the goal must be taken into account. Heat flux q_{cg} is convenient to use as a normalizing heat flux q_n when aiming to highlight the change of the complex heat flux relationship since it does not obtain a negative value in the process of the droplet phase change (Fig. 4 a). The dynamics of the relation between heat fluxes q_{cl}/q_{cg} (Fig.10 a) describes the input of the complex heating process components into the change of the droplets' thermal state. At the initial stage of the phase change $\bar{q}_{cl} > 1$, therefore this relation indicates the additional input of condensation heat. The input of the absorbed radiation should also be considered; in this case it is indicated by $\bar{q}_r$ (Fig. 11 a). At the moment the condensation regime changes to evaporation $\bar{q}_{cl}(Fo \equiv Fo_{ko}) = 1$ and from this moment on, the water within the droplet is heated by the absorbed radiation and the convective heat that does not participate in water surface evaporation. At the time $\bar{q}_{cl}(Fo) = 0$, all convective heat participates in the water evaporation process. Later, a part of the absorbed radiation, which was directed to the surface by internal convection, starts to participate in the evaporation process. The condition $\bar{q}_{cl}(Fo \equiv Fo_e) = \bar{q}_r(Fo \equiv Fo_e)$ indicates the start time Fo_e of the equilibrium evaporation, and later the proportion between $\bar{q}_{cl}(Fo > Fo_e)$ *and* $\bar{q}_r(Fo > Fo_e)$ is defined by the cooling droplet enthalpy joining the water evaporation process and the qualitative change of the radiation local heat flux at the final stage of evaporation. The dynamics of the relation between heat fluxes q_f/q_{cg} (Fig. 10 b) describes the specific features

of the change in energy origin of the heat participating in the phase changes at the droplets' surfaces. In order to evaluate the dynamics of the heat flux at the droplet's surface, it is convenient to consider the dynamics of the parameters $\bar{q}(Fo) \equiv q(Fo)/q_0$ defined by heat flux time functions q(Fo) and the initial heat flux relation (Fig. 12 and 13). The following functions define such universal qualitative diagrams of the droplet phase change process variation: function $\bar{q}_{cg}(Fo) \equiv q_{cg}(Fo)/q_{cg,0}$ describes the variation of convection heat flux (Fig. 12 a); function $\bar{q}_{cl}(Fo)$ describes the variation of convective heat flux in a droplet (Fig. 12 b); function $\bar{q}_f(Fo)$ the variation of the phase change heat flux at the surface of the droplet; function $\bar{q}_r(Fo)$ describes the variation of the radiation heat flux absorbed in a semi-transparent droplet.

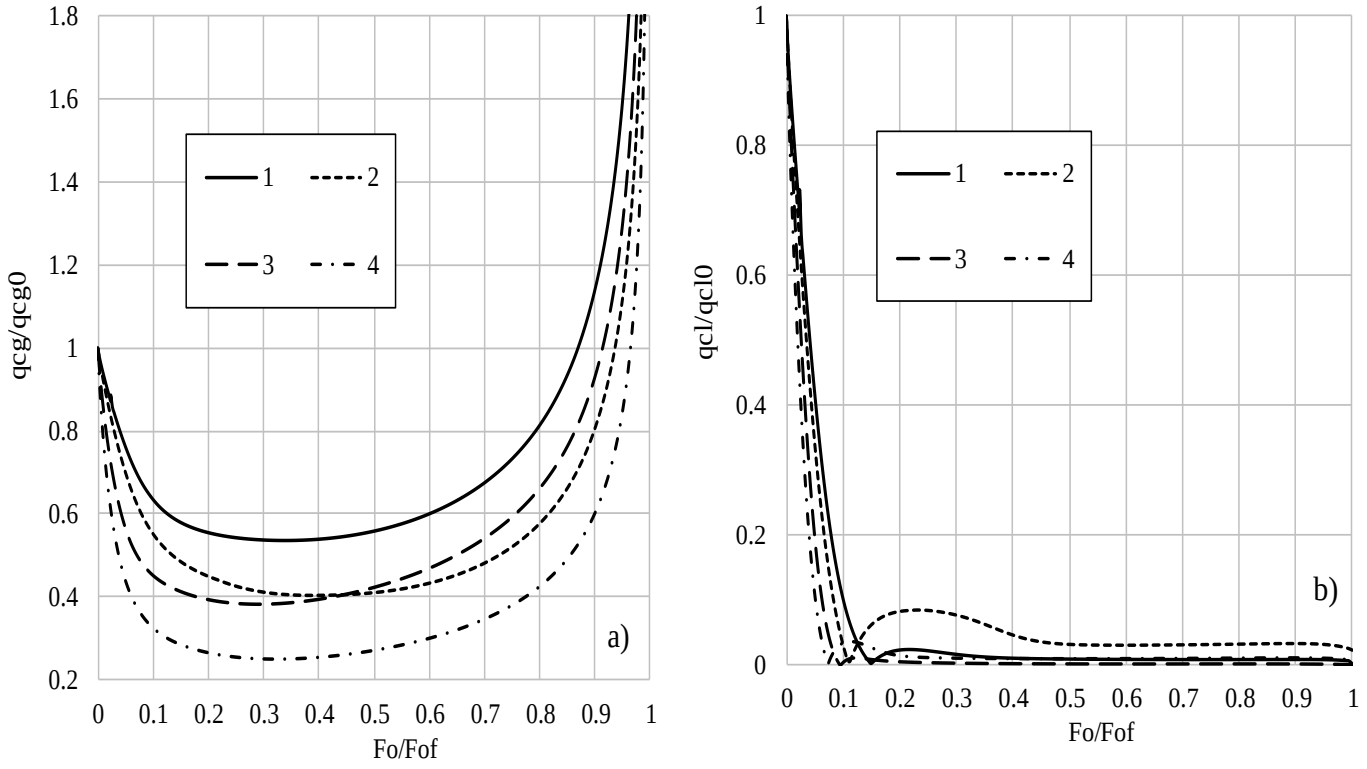

Fig. 12. The variation of $q_{cg}/q_{cg,0}$ ratio (a) and $q_{cl}/q_{cl,0}$ ratio (b) of heat flux in the process of water droplets phase change in the case of complex heating. $R_0 \times 10^6$, m: (1, 3) 25, (2, 4) 100; T_g, K (1, 2) 1133, (3, 4) 678; $T_{l,0} = 306$ K; $w_{l,0} = 65$ m/s; $w_g = 15$ m/s; $\bar{p}_v = 0.2$.

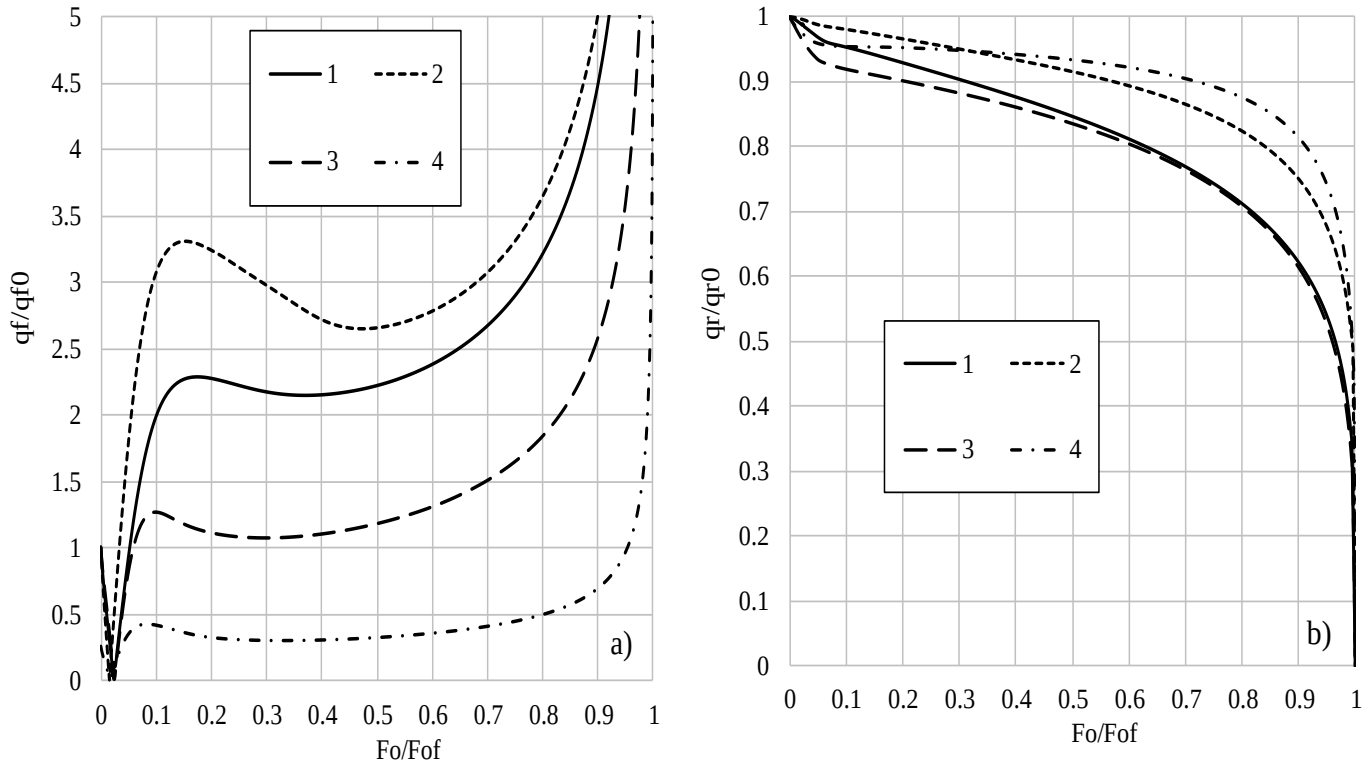

Fig. 13. The variation of $q_f/q_{f,0}$ ratio (a) and $q_r/q_{r,0}$ ratio (b) of heat flux in the process of water droplets phase change in the case of complex heating. $R_0 \times 10^6$, m: (1, 3) 25, (2, 4) 100; T_g, K (1, 2) 1133, (3, 4) 678; $T_{l,0} = 306$ K; $w_{l,0} = 65$ m/s; $w_g = 15$ m/s; $\bar{p}_v = 0.2$.

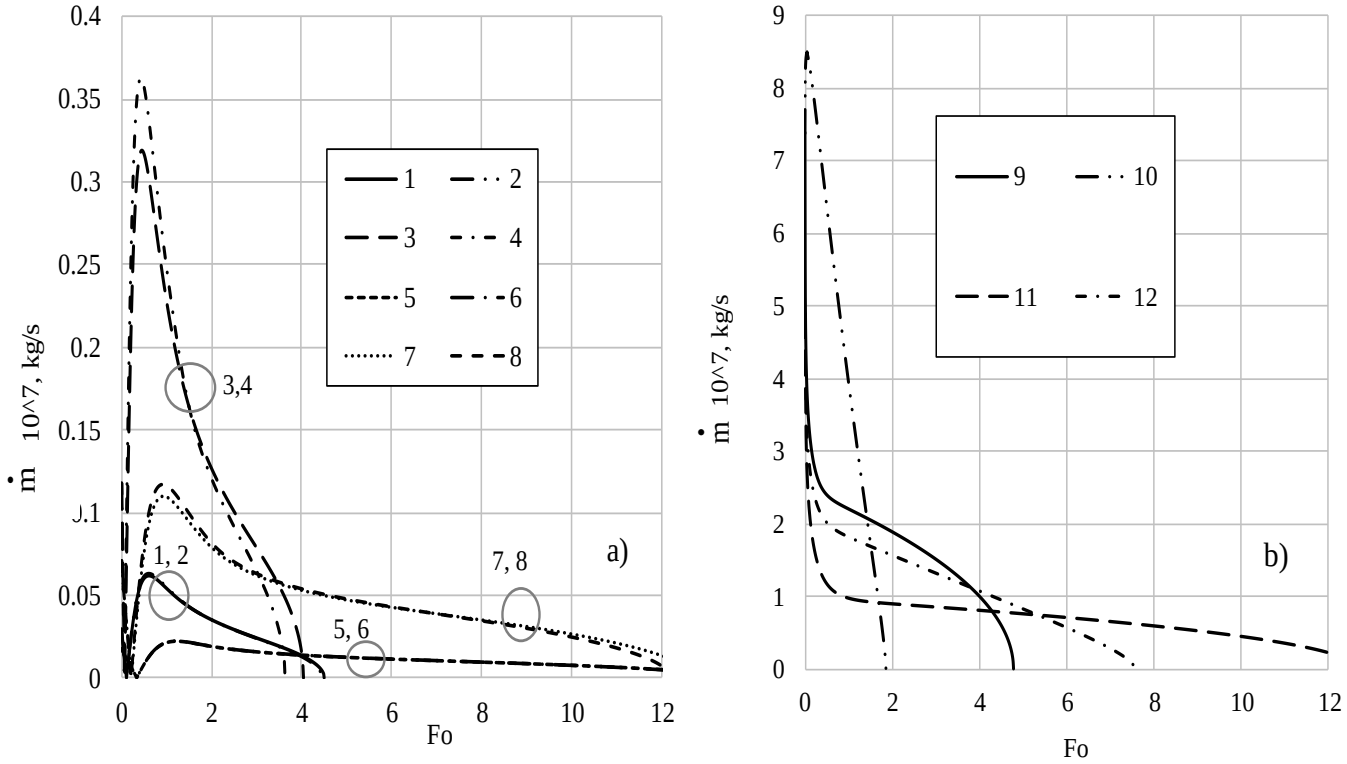

Fig. 14. Vapor flow rate at the surfaces of small and average size (a) and large (b) droplets dependency on the heating process: (1, 3, 5, 7) convective heating, (2. 4, 6, 8) complex heating – convection and radiation, (9, 11) conductive heating, (10, 12) complex heating – conduction and radiation; $\dot{m}_0 \times 10^7$, kg/s: (1, 2) 0.0294, (3, 4) 0.1178, (5, 6) 0.0177, (7, 8) 0.0708, (9, 10) 7.388, (11, 12) 4.896; $R_0 \times 10^6$, m: (1, 2, 5, 6) 25, (3, 4, 7, 8)

100; (9, 10) 1500, (11, 12) 1600; T_g, K (1-4, 9, 10) 1133, (5-8, 11, 12) 678; $T_{l,0}$, K: (1-8) 306, (9-12) 358; $\bar{p}_v$: (1-8) 0.2, (9-12) 0; $w_{l,0}$, m/s: (1-8) 65, (9-12) 0; w_g, m/s: (1-8) 15, (9-12) 0.

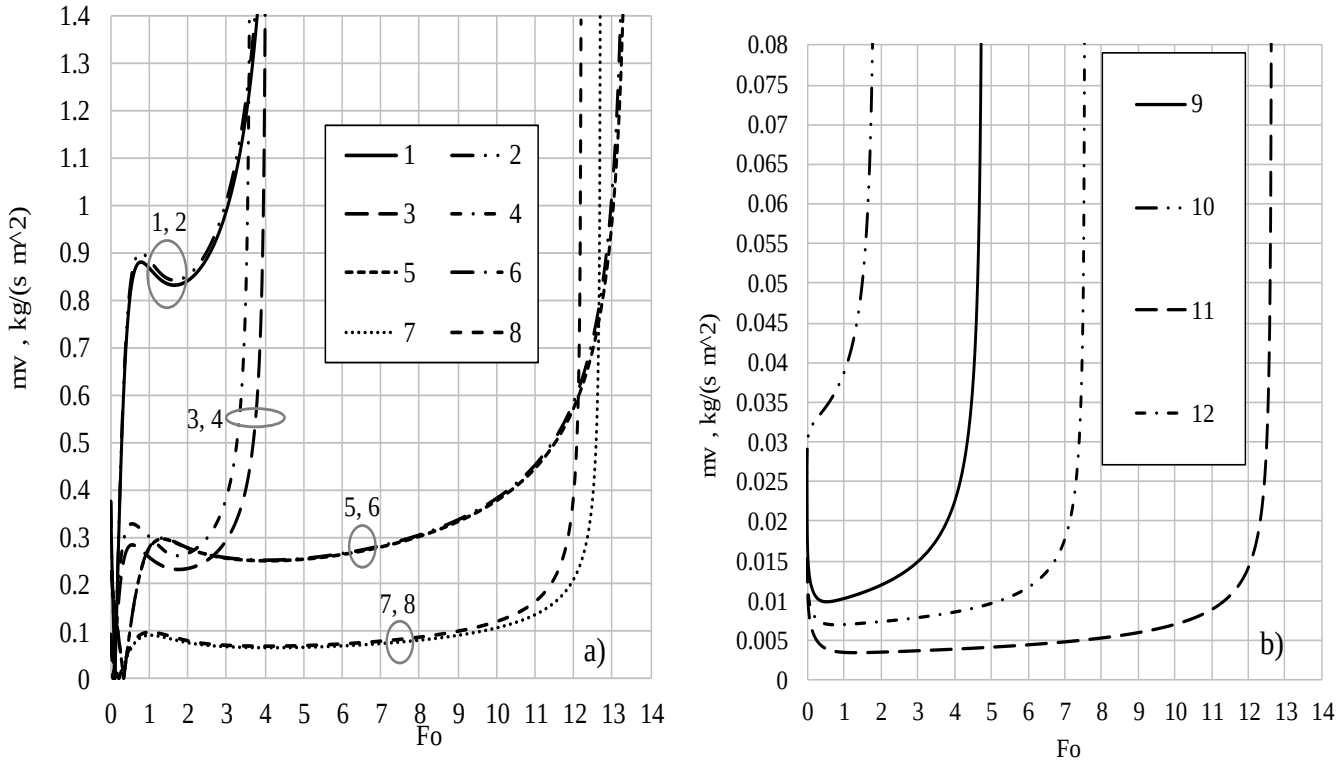

Fig. 15. Vapor flux at the surfaces of small and average size (a) and large (b) droplets dependency on the heating process. $m_{g,0}$, kg/(m^{2}s): (1, 2) 0.3748, (3, 4) 0.0937, (5, 6) 0.2253, (7, 8) 0.0563, (9, 10) 0.02613, (11, 12) 0.01522. Boundary conditions as in Fig. 14.

The characteristics of droplet thermal and energy states as well as phase change determined by the interaction of complex transfer processes define the parameter for water vapor flow rate $\dot{m}_v$, kg/s at the droplet surface, which is important to water dispersion technologies. The intensity of vapor flow is defined by vapor flux m_v kg/(m^{2}s). The vapor flow rate at the surfaces of the droplets approaches the zero value from the initial value $\dot{m}_{v,0}$ in the process of phase change when the droplets evaporate (Fig. 14), and the vapor flux increases quickly at the final stage of evaporation (Fig. 15). The initial vapor flux is defined by the temperature of the dispersed water, the droplet dispersity, and the air humidity. In the condensation regime, the vapor flux at the surface of cold water droplets decreases to zero, while in the transitional regime, it increases to the value $m_{v,e}$, which is also influenced by the droplet heating process. At the beginning of equilibrium evaporation, $m_{v,e}$, kg/(s m^2) is 0.8724, 0.8995, 0.2815, 0.3274, 0.2951, 0.2973, 0.09192 and 0.0985 for boundary conditions (1–8), respectively (Fig. 15 a). At the beginning of the equilibrium evaporation, the vapor flow rate $\dot{m}_e \cdot 10^7$, kg/s is 0.0615, 0.0614, 0.3171, 0.3455, 0.0221, 0.02212, 0.1097 and 0.1158, respectively (Fig. 14 b). Warm water droplets instantly reach equilibrium evaporation and in their case $\dot{m}_e \equiv \dot{m}_0$ (Fig. 14 b) and $m_{v,e} \equiv m_{v,0}$ (Fig. 15 b). At the initial stage of equilibrium evaporation, the increase in vapor flow rate is defined by the enthalpy of the cooling droplets participating in the water evaporation process; however, it is also suppressed by the weakening intensity of the convective heating, which is defined by the decrease in droplet slipping. The increase of the vapor flow rate is also directly defined by the decrease of the droplet's surface area. The result of these factors is the extreme points formed in the diagrams of the vapor flux variation, and the rapid increase in the vapor flow rate at the final stage of droplet evaporation is defined by the decrease of the droplets' surface area.

The equilibrium evaporation velocity of the large water droplets was experimentally investigated in [17] in the case of complex heating. The experiment was performed in an original test section where the water was fed into the centre of a chamber heated up to a temperature of 405–860 ^{0}C via a capillary system. An evaporating water droplet of 600–2900 μm diameter was formed at the outlet of a 3 mm diameter copper

capillary tube. The droplet was heated by the radiation from the chamber walls and the convective heat of the air-water vapor mixture flowing around the chamber was extracted. The extraction of the air-water vapor flow helped to satisfy the condition necessary to the flow regime so that the calculated Reynolds number Re<3. The water feeding the evaporating droplet was heated to such a temperature that an additional 25–30 ^{0}C from the capillar would not change the droplet temperature measured by a thermocouple. After ensuring the stability of the 30–50 times enlarged projection of the illuminated droplet on a screen, the velocity of the droplet evaporation was assumed to be the measured feed water flow rate [17]. The experimental results have been compared to the modeling results of large water droplet evaporation in 1133K and 678 K temperature environments in the dependence of the equilibrium evaporation intensity $\dot{m}_e$ on their radius (Fig. 16 a). The diagrams of functions $\dot{m}(R)$were drawn based on the functions $R(\mathrm{Fo})$ (Fig. 16 b) calculated during the modeling of the droplet evaporation process and based on the evaporation intensity $\dot{m}_i$ calculated for corresponding Fo_i moments in time; the experimental points were taken based on results from the work in [17].

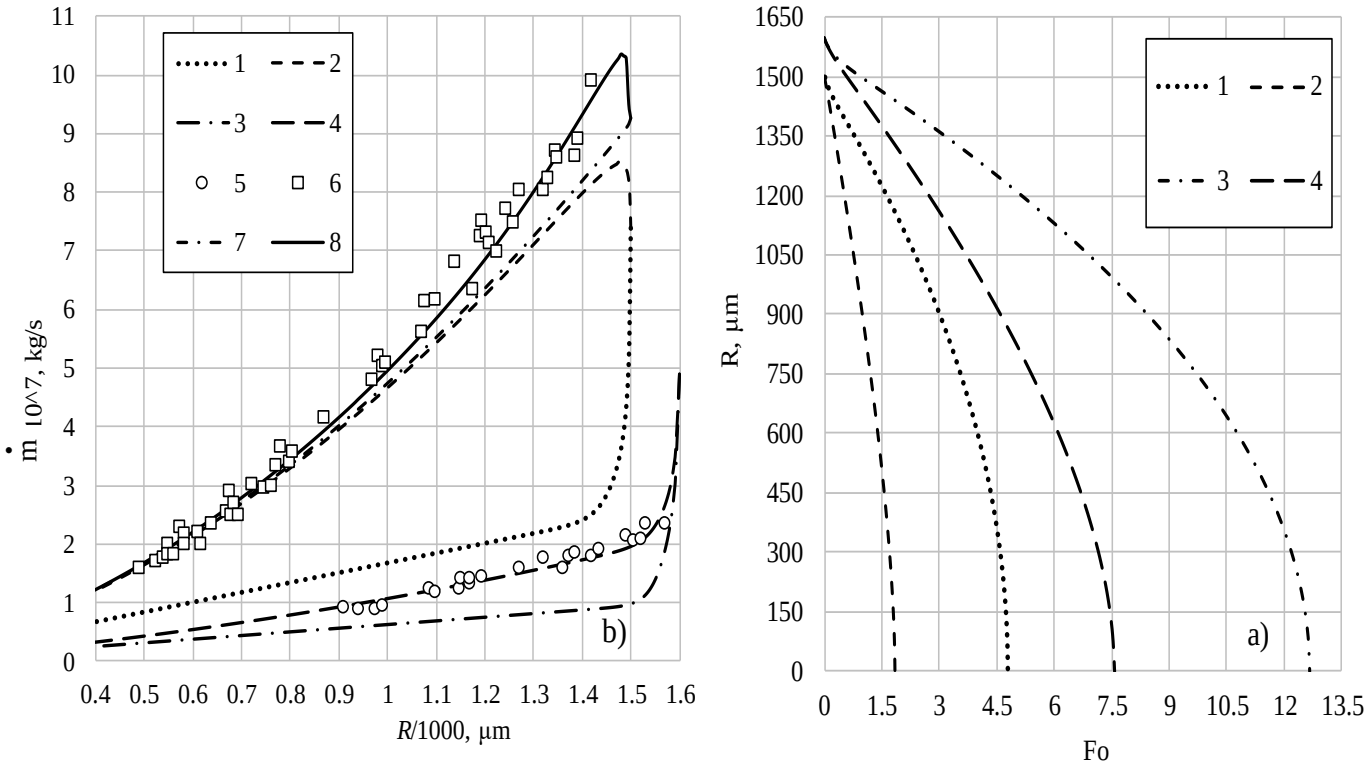

Fig. 16. The influence of the heating process on the vapor flow of large water droplets at their surfaces (a) and for the radius dynamics (b): (1, 3) conductive heating, (2, 4, 7) complex heating – conduction and radiation, (5, 6, 8) complex heating – conduction radiation and weak convection; $R_0\times10^6$, m: (1, 2, 7, 8) 1500, (3, 4) 1600; T_g, K (1, 2, 6-8) 1133, (3-5) 678; $T_{l,0}$, K: (1-4) 358, (5, 6) T_e, (7, 8) 362; Re_0 (1-4, 7) 0, (5, 6) $\mathrm{Re}<3$ [17], (8) 1.7; $\bar{p}_v\approx0$; the lines represent the modeling results; the points represent the experimental results [17].

While modeling the experimental boundary conditions, the temperature of the radiation source T_{sr} was assumed to be equal to the air temperature T_g. However, the initial droplet temperature $T_{l,0}$ was estimated intuitively, and there were still the uncertainties considering the humidity of the air-water vapor flow extracted from the chamber and the droplet flow regime. During the experiments, the air humidity was not set. During the modeling, the assumption $\bar{p}_v\approx0$ was used. In the modeling, the possible experimental droplet flow regimes were defined with boundary values $\mathrm{Re}_{0,\min}\approx0$ and $\mathrm{Re}_{0,\max}\approx3$ for the Reynolds number $\mathrm{Re}=2R\rho_g w_g/\gamma_{vg}$. When modeling the evaporation of a conductively heated droplet (Fig. 16 a, curves 1, 3), $\mathrm{Re}_0=0$ and T_{sr}=0; in the

case of complex heating with conductivity and radiation (Fig. 16 a, curves 2, 4, 7), $\mathrm{Re}_0 = 0$ and $T_{sr}=T_g$; in the case of complex heating with convection and radiation (Fig. 16 a, curve 8) $\mathrm{Re}_0 = 1.7$ and $T_{sr}=T_g$.

At first, the modeling results were compared with the afore-mentioned calculated evaporation mass flow rate of the modeled large 358 K temperature water droplets, heating them using conduction, and in the case of complex heating (Fig. 16, curves 1–4, points 5, 6). The droplet heating process had a strong influence on their evaporation intensity. At the relatively low 678 K temperature under the influence of radiation, the velocity of droplet evaporation increases to twice the value from conductive heating (Fig. 16, curves 3 and 4). In this case, the water droplets of 358 K temperature cool down quickly to the equilibrium evaporation temperature, and after that the diagram of the function $\dot{m}_{e,R} \equiv \dot{m}\left[R(\tau)\right]$ defining their evaporation intensity variation practically coincides with the experimental results (Fig. 16, curve 4 and 5 points). For the high temperature of 1133 K in the radiation environment, the equilibrium evaporation of large droplets is more rapid by several times compared to the evaporation of conductively heated droplets (Fig. 16, curves 1 and 2). In the case of complex heating, the water droplets of 358 K temperature warm up at first, and their evaporation intensity increases to that for equilibrium evaporation; however, the diagram curve $\dot{m}_{e,R}$ is a little lower compared to the experimental results (Fig. 16, curve 2, data points 6). The water droplets of 362 K temperature evaporate in the equilibrium manner, and their curve for $\dot{m}_{e,R}$ in the diagram is closer to the experimental results; however, the level of experimental results is not reached for the droplets larger than 1.5 mm diameter (Fig. 16, curve 7, data points 6). In the case of heating with convection ($\mathrm{Re}_0 = 1.7$) and radiation, the water droplets of 362 K temperature warm up rapidly to the equilibrium evaporation temperature. After that the function $\dot{m}_{e,R}$ for their mass flow rate practically coincides with the experimental results (Fig. 16, curve 8, data points 6).

4 CONCLUSIONS

Condensation, transitional evaporation and equilibrium evaporation regimes are clearly noticed in the wet gas flow in the process of water droplet phase change. The characteristics of dispersed water phase changes are defined by the specific features of droplet thermal and energy state change. In the transitional phase change regime, they are defined by the temperature of the dispersed water, and at the equilibrium evaporation regime, the factors of gas temperature and humidity are important.

When the temperature of the dispersed water is lower than the dew point, the cycle of droplet phase change starts with the condensation regime. The duration of the condensation regime is clearly defined by the droplet's warm up to the dew point temperature. The end of the transitional phase change regime is defined based on water droplet warming up to the thermal state that ensures equilibrium evaporation; it is defined by temperature $T_{l,e}$. The process of droplet heating plays an important role when defining the equilibrium evaporation temperature $T_{l,e}$. In the case of convective heating, temperature $T_{l,e}$ is defined by the instantaneous highest temperature $T_{R,\max}$ of the droplet's surface, while in the case of complex heating it is the average instantaneous highest temperature $T_{m,\max}$ of the droplet's mass.

The parameter $\bar{T}_{l,0} \equiv T_{l,0} / T_{l,e}$ which is expressed through the ratio of water temperature and droplet equilibrium evaporation temperature defines the thermal state variation of droplets. When $\bar{T}_{l,0} < 1$, the water is assumed to be relatively cold, and its droplets warm up to temperature $T_{l,e}$ in the transitional phase change regime. When $\bar{T}_{l,0} > 1$, the water is assumed to be relatively warm, and its droplets cool down during equilibrium evaporation.

The droplet energy state variation is defined by the dynamics of the heat fluxes at the droplet's surface for which the parameter $\bar{q}_n$ expressed through heat flux ratios q_{cg}/q_n q_r/q_n, q_{cl}/q_n, q_f/q_n is important. The normalizing heat flux q_n is chosen based on the goal of the energy state assessment. The variation in interrelation between heat fluxes becomes clear when the heat flux q_{cg} obtaining no negative value in the process of the droplet phase change is used instead of normalizing heat flux q_n. The common characteristics of heat flux variation become clear in the droplet phase change regimes when the initial heat flux q_0 are used instead of normalizing parameter q_n.

When water is dispersed into the high temperature flue gas of a biofuel furnace, the heating of the droplets is defined by radiation and droplet slipping factors. Traditional technologies of flue gas heat utilization cool down the flue gas, yet the flue gas temperature before a condensing shell and tube heat exchanger is higher than the dew point temperature and the humidity is still high. For this reason, the thermal state of the equilibrium evaporation of the dispersed droplets is defined by the humidity of the flue gas, and the condensation regime duration in the transitional phase change regime becomes more significant. The effect of the radiation of a relatively low temperature in the flue gas on the transfer processes becomes weaker, and the droplet slipping factor becomes more significant. A higher slipping velocity of droplets means more intensive convective heating; however, the water circulation in the droplets is more intensive due to friction forces, and therefore heat removal to the centre of the droplet intensifies. This gives the necessary conditions for the diminishing of the warming up of the droplet surface and for the duration of the condensation regime to become longer, which is convenient when talking about the increased efficiency of the utilization of phase change heat from the biofuel flue gas.

REFERENCES

[1] A Abdel-Salam A. H., Simmson J. C., State-of-the-art in liquid desiccant air conditioning equipment and systems, *Renewable and Sustainable Energy Reviews*, Vol 58, pp. 1152-1183, 2016. https://doi.org/10.1016/j.rser.2015.12.042

[2] Bucklin J. M., Mitigation of industrial hazards by water spray curtains, *Journal of Loss Prevention in the Process Industries*, Vol. 50, pp. 91-100, 2017. https://doi.org/10.1016/j.jlp.2017.08.007

[3] Paepe W., Carrero M., Bram S., Contino F., Parente A., Waste heat recovery optimization in micro gas turbine applications using advanced humidified gas turbine cycle concepts, *Applied Energy*, Vol. 207, pp. 218-229, 2017. https://doi.org/10.1016/j.apenergy.2017.06.001

[4] Hsieh S., Luo S., Droplet impact dynamics and transient heat transfer of a micro spray system for power electronics devices, *International Journal of Heat and Mass Transfer*, Vol 92, pp 190-205, 2016. https://doi.org/10.1016/j.ijheatmasstransfer.2015.08.099

[5] P. L. C. Lage, C. M. Hackenberg, R. H. Rangel, Nonideal Vaporization of Dilating Binary Droplets with Radiation Absorption**,** *Combustion and Flame*, Vol. 101, pp. 36–44, 1995. https://doi.org/10.1016/0010-2180(94)00191-T

[6] L. A Dombrovsky, S. S Sazhin, E. M. Sazhina, G. Feng, M. R. Heikal, M. E. A. Bardsley, Heating and evaporation of semi-transparent diesel fuel droplets in the presence of thermal radiation, *Fuel*, Vol. 80, pp. 1535–1544, 2001. https://doi.org/10.1016/S0016-2361(01)00025-4

[7] G. Miliauskas, Regularities of unsteady radiative-conductive heat transfer in evaporating semi-transparent liquid droplets, *International Journal of Heat and Mass Transfe*r, Vol. 44, pp. 785–798, 2001. https://doi.org/10.1016/S0017-9310(00)00127-7

[8] C. C. Tseng, R. Viskanta, Enhancement of water droplet evaporation by radiation absorption, *Fire Safety Journal*, Vol. 41, pp. 236-247, 2006. https://doi.org/10.1016/j.firesaf.2006.01.001

[9]. M. Q. Brewster, Evaporation and condensation of water mist/cloud droplets with thermal radiation, *International Journal of Heat and Mass Transfe*r, Vol. 44, pp. 785–798, 2015. https://doi.org/10.1016/j.ijheatmasstransfer.2015.03.055

[10] G. M. Hale, M. R Query, Optical constants of water in the 200-nm to 200-μm wavelength region, *Applied Optics*, Vol. 12, pp. 555–562, 1973. https://doi.org/10.1364/AO.12.000555

[11] G. M. Hale, M. R Query, A.N. Rusk, D. Williams, Influence of temperature on the spectrum of water, *J. Opt. Soc. Am.*, Vol. 62, pp. 1103–1108, 1972. https://doi.org/10.1364/JOSA.62.001103

[12] W. A. Sirignano, Fluid Dynamics and Transport of Droplets and Sprays, *Cambridge University Press*, p. 311, 1999.

[13] S. S. Sahin, Droplets and Sprays, *Springer*, p. 352, 2014.

[14] B. Abramzon, W. A. Sirignano, Droplet vaporization model for spray combustion calculations, *International Journal of Heat and Mass Transfer*, Vol 32, pp 1605-1618, 1989. https://doi.org/10.1016/0017-9310(89)90043-4

[15] Miliauskas G., Maziukiene M., Ramanauskas V., Puida E., The defining factors of the phase change cycle of water droplets that are warming in humid gas, *International Journal of Heat and Mass Transfer*, Vol 113, pp 683-703, 2017. https://doi.org/10.1016/j.ijheatmasstransfer.2017.05.129

[16] A. V. Kuzikovskij, Dynamics of spherical particle powerful optical field, *Izv. VUZ Fizika*, Vol. 5, pp. 89–94, 1970.

[17] V.M. Ivanov, E.V. Smirnova. Experimental research of liquid droplets evaporation velocity in non-moving high temperature environment. *Tr. IGI*, Vol. 19, pp. 46-58, 1962.